SHEAR STRENGTH OF FRACTURE IN SANDSTONE UNDER TRUE TRIAXIAL STRESSES

Piyanat Kapang

A Thesis Submitted in Partial Fulfillment of the Requirements for the Degree of Master of Engineering in Geotechnology

Suranaree University of Technology

Academic Year 2012

กำลังเฉือนของรอยแตกในหินทรายภายใต้ความเค้นในสามแกนจริง

นายปิยะณัติ ค่าแพง

วิทยานิพนธ์นี้เป็นส่วนหนึ่งของการศึกษาตามหลักสูตรปริญญาวิศวกรรมศาสตรมหาบัณฑิต

สาขาวิชาเทคโนโลยีธรณี

มหาวิทยาลัยเทคโนโลยีสุรนารี

ปีการศึกษา 2555

SHEAR STRENGTH OF FRACTURE IN SANDSTONE UNDER TRUE TRIAXIAL STRESSES

Suranaree University of Technology has approved this thesis submitted in partial fulfillment of the requirements for a Master's Degree.

Thesis Examining Committee

____

(Assoc. Prof. Kriangkrai Trisarn)

Chairperson

____

(Assoc. Prof. Dr. Kittitep Fuenkajorn)

Member (Thesis Advisor)

____

(Dr. Decho Phueakphum)

Member

____

(Prof. Dr. Sukit Limpijumnong)

Vice Rector for Academic Affairs

____

(Assoc. Prof. Flt. Lt. Dr. Kontorn Chamniprasart)

Dean of Institute of Engineering

ปิยะณัติ ค่าแพง : กำลังเฉือนของรอยแตกในหินทรายภายใต้ความเค้นในสามแกนจริง(SHEAR STRENGTH OF FRACTORE IN SANDSTONE UNDER TRUE TRIAXIAL STRESSES) อาจารย์ที่ปรึกษา : รองศาสตราจารย์ ดร.กิตติเทพ เฟื่องขจร, 66 หน้า.

การทดสอบกำลังรับแรงเฉือนในสามแกนจริงได้ดำเนินการเพื่อตรวจสอบค่ากำลังรับแรงเฉือนของรอยแตกที่ถูกจำลองขึ้นในหินทรายสามชนิดในประเทศไทย โครงกดทดสอบแบบหลายแกนได้ถูกใช้เพื่อให้ความเค้นล้อมรอบ(σ_p และ σ_o) ต่อตัวอย่างที่มีลักษณะเป็นก้อนสี่เหลี่ยมผืนผ้า ขนาด 76×76×126 มิลิเมตร ระนาบของรอยแตกที่ถูกจำลองขึ้นทำมุมเอียง 59.1 องศากับความเค้นหลักในแนวแกน ผลจากการทดสอบแสดงให้เห็นว่าความเค้นล้อมรอบที่ขนานกับระนาบรอยแตกสามารถลดกำลังรับแรงเฉือนของรอยแตกได้ ภายใต้ความเค้นตั้งฉากเดียวกันรอยแตกที่อยู่ภายใต้ความเค้นล้อมรอบที่ขนานกับระนาบรอยแตกที่มีค่าสูง จะมีการขยายตัวของรอยแตกมากกว่ารอยแตกที่อยู่ภายใต้ความเค้นล้อมรอบที่มีค่าต่ำ จากเกณฑ์ของคูลอมบ์ค่ามุมเสียดทานลดลงในเชิงเอกซ์โพเนนเชียลเมื่อทำการเพิ่มอัตราส่วนของความเค้นล้อมรอบ (σ_p/σ_o) และค่าความเค้นยึดติดจะมีค่าลดลงเมื่อเพิ่มค่าความเค้นล้อมรอบที่ขนานกับระนาบรอยแตก ค่าความเค้นล้อมรอบ σ_p จะไม่ส่งผลกระทบต่อค่ามุมเสียดทานพื้นฐานของรอยแตกพื้นผิวเรียบ จากผลการทดสอบกำลังรับแรงเฉือนของรอยแตกภายใต้ $\sigma_p = 0$ จะมีความสัมพันธ์กันอย่างดีกับผลการทดสอบกำลังรับแรงเฉือนแบบโดยตรงซึ่งระบุว่าเมื่อมีการให้แรงด้านข้างในทิศทางที่ขนานกับระนาบรอยแตก (σ_p) จะเกิดความเครียดภายในพื้นผิวรอยแตกคือมีการบัวตัวของผนังรอยแตกเข้าไปในรอยเปิดเผยดังนั้นจึง เป็นผลให้เกิดการเฉือนหรือการเลื่อนไหลได้ง่ายกว่ากรณีที่ไม่มีความเค้นล้อมรอบ

สาขาวิชา <u>เทคโนโลยีธรณี</u>	ลายมือชื่อนักศึกษา ______________
ปีการศึกษา 2555	ลายมือชื่ออาจารย์ที่ปรึกษา ______________

PIYANAT KAPANG : SHEAR STRENGTH OF FRACTURE IN SANDSTONE UNDER TRUE TRIAXIAL STRESSES. THESIS ADVISOR : ASSOC. PROF. KITTITEP FUENKAJORN, Ph.D., P.E., 66 PP.

JOINT SHEAR STRENGTH/TRUE TRIAXIAL STRESSES/FRICTION ANGLE/COHESION

True triaxial shear tests have been performed to determine the peak shear strengths of tension-induced fractures in three Thai sandstones. A polyaxial load frame is used to apply mutually perpendicular lateral stresses (σ_p and σ_o) to the 76×76×126 mm rectangular block specimens. The normal of the fracture plane makes an angle of 59.1° with the axial (major principal) stress. Results indicate that the lateral stress that is parallel to the fracture plane (σ_p) can significantly reduce the peak shear strength of the fractures. Under the same normal stress (σ_n) the fractures under high σ_p dilate more than those under low σ_p. According to the Coulomb criterion, the friction angle decreases exponentially with increasing σ_p/σ_o ratio and the cohesion decreases with increasing σ_p. The lateral stress σ_p has insignificant effect on the basic friction angle of the smooth saw-cut surfaces. The fracture shear strengths under $\sigma_p = 0$ correlate well with those obtained from the direct shear tests. It is postulated that when the fractures are laterally confined by σ_p, their asperities are strained into the aperture, and are sheared off more easily compared to those under unconfined condition.

School of Geotechnology____ Student's Signature______________________

Academic Year 2012 Advisor's Signature______________________

ACKNOWLEDGMENTS

I wish to acknowledge the funding supported by Suranaree University of Technology (SUT).

I would like to express my sincere gratitude thanks to Assoc. Prof. Dr. Kittitep Fuenkajorn for his valuable guidance and efficient supervision. I appreciate for his strong support, encouragement, suggestions and comments during the research period. My heartiness thanks to Assoc. Kriangkrai Trisarn and Dr. Decho Phueakphum for their constructive advice, valuable suggestions and comments on my research works as thesis committee members. Grateful thanks are given to all staffs of Geomechanics Research Unit, Institute of Engineering who supported I work.

Finally, I would like to thank beloved parents for their love, moral support and constant encouragement.

Piyanat Kapang

TABLE OF CONTENTS

Page

TABLE OF CONTENTS (Continued)

Page

TABLE OF CONTENTS (Continued)

Page

LIST OF TABLES

Table **Page**

LIST OF FIGURES

Figure **Page**

LIST OF FIGURES (Continued)

Figure **Page**

LIST OF FIGURES (Continued)

Figure **Page**

SYMBOLS AND ABBREVIATIONS

σ_1	=	Maximum principal stress (axial stress)
σ_p	=	Lateral stress (parallel plane stress)
σ_o	=	Lateral stress (on plane stress)
σ_n	=	Normal stress
τ	=	Shear stress
d_s	=	Shear displacement
d_n	=	Normal displacement
d_1	=	Axial displacement (monitored in direction of σ_1)
d_o	=	Lateral displacement (monitored in direction of σ_o)
c^*	=	Apparent cohesion
ϕ^*	=	Apparent friction angle
β	=	Angle between σ_1 and σ_n
α	=	Empirical constant (friction angle in case of $\sigma_p = 0$)
κ	=	Empirical constant (cohesion in case of $\sigma_p = 0$)
ψ	=	Empirical constant
ξ	=	Empirical constant
JRC	=	Joint roughness coefficient
PKSS	=	Phu Kradung sandstone
PPSS	=	Phu Phan sandstone
PWSS	=	Phra Wihan Sandstone

CHAPTER I

INTRODUCTION

1.1 Background and rationale

Direct shear testing (e.g., ASTM D5607-08) has widely been used to determine the peak and residual strengths of the rock fractures. Its test configurations however pose some disadvantages that the magnitudes of the applied normal stress are limited by the uniaxial compressive strength of the rock and that the fractures are sheared under unconfined conditions. The triaxial shear testing (Brady & Brown, 2006; Jaeger et al., 2007) has been developed to simulate the frictional resistance of rock fractures under confinements. The cylindrical rock core containing an inclined fracture or weakness plane can be axially loaded in a triaxial pressure cell with a wide range of applied confining pressures. The normal stress at which the shear strengths are measured can be controlled by the applied axial stress and confining pressures. Determination of the fracture shear strengths under true triaxial stresses where the shear sliding occurs under anisotropic stresses ($\sigma_1 \neq \sigma_2 \neq \sigma_3$) has not been attempted.

1.2 Research objectives

The objective of this study is to experimentally determine the shearing resistance of fractures in sandstone specimens under true triaxial stresses. The effort involves performing true triaxial shear tests on tension-induced fractures and smooth saw-cut surfaces by using a polyaxial load frame. The conventional direct shear tests are also performed to compare their results with those of the true triaxial stresses.

Empirical equations representing the cohesion and friction angle as a function of with the applied multi-axial stresses are derived and incorporated into the Coulomb criterion.

1.3 Research methodology

The research methodology shown in Figure 1.1 comprises 6 steps; including literature review, sample preparation, laboratory testing, development of mathematical relations, discussions and conclusions, and thesis writing.

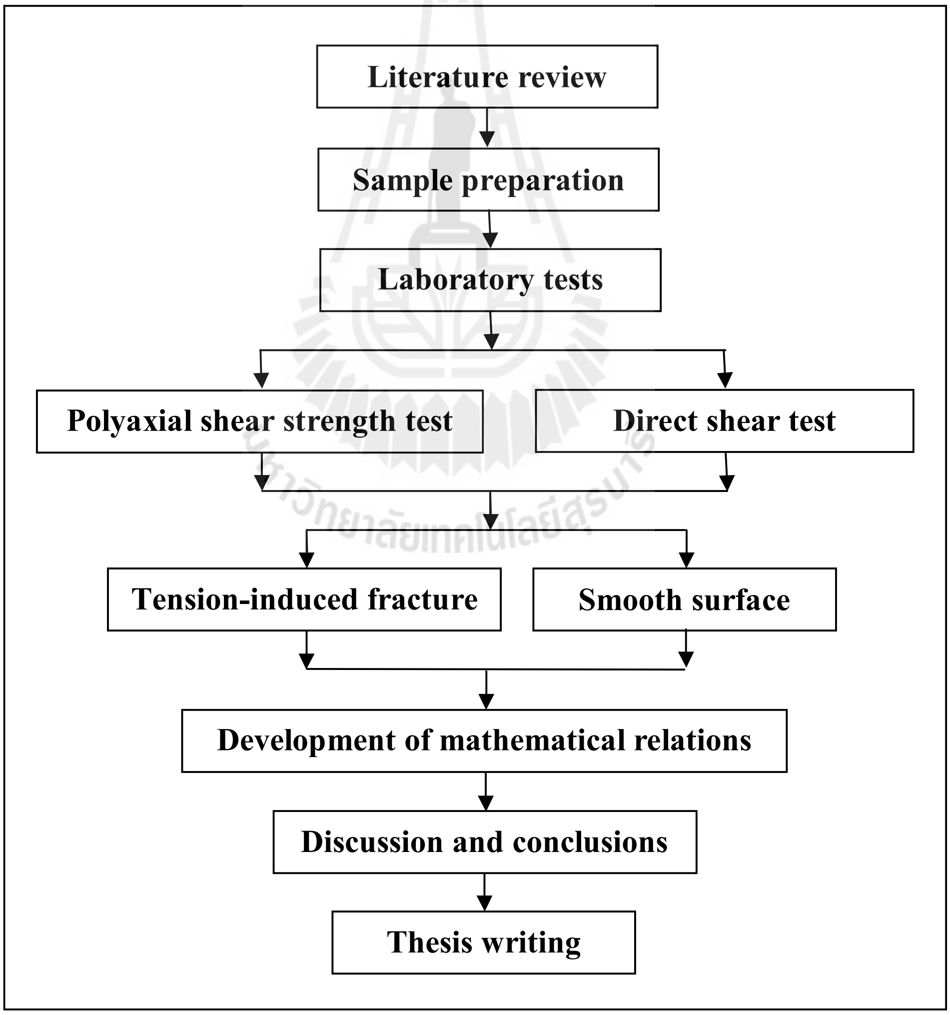

Figure 1.1 Research methodology.

1.3.1 Literature review

Literature review has been carried out to improve an understanding of joint shear strength in conventional method, true triaxial or polyaxial stress as affected by the lateral stress and new equations development.

1.3.2 Sample preparation

The specimens used for the true triaxial shear tests are prepared from the Phu Kradung, Phu Phan and Phra Wihan sandstones (hereafter designated as PKSS, PPSS and PWSS). They are cut to obtain rectangular blocks with nominal dimensions of 76×76×126 mm^3. A line load is applied to obtain a tension-induced fracture diagonally across the sandstone block. The asperity amplitudes on the fracture planes are measured from the laser-scanned profiles along the shear direction. The maximum amplitudes are used to estimate the joint roughness coefficients (JRC) of each fracture based on Barton's chart (Barton, 1982). For the specimens with the saw-cut surface have been prepared to rectangular block with dimensions of 76×76×126 mm^3. All specimens are oven-dried before testing. For the direct shear test specimens a line load is applied to obtain a tension-induced fracture at the mid-section of the 100×100×160 mm^3 sandstone blocks. The fracture area is 100×100 mm^2.

1.3.3 Laboratory testing

A polyaxial load frame (Fuenkajorn and Kenkhunthod, 2010; Fuenkajorn et al., 2012) is used to apply true triaxial stresses to the specimens (Figure 1.2). Neoprene sheets are used to minimize the friction at all interfaces between the loading plate and the rock surface, before the testing specimen is not tension induced have put in the polyaxial load frame for determine friction of interface. The testing have been divided two series. First set of tests parallel plane stresses (σ_p) is proportioned on plane stresses (σ_o), σ_p/σ_o is varied from 0, 0.5, 1, 2, 3 and 4 while σ_1 maximum principal stresses are increased until peak shear stresses are occurred. Second set of tests σ_p is maintained constant, σ_o is varied from 0.6 to 5 MPa while σ_1 is increased until peak shear stresses is occurred. From two series testing, before applied loading the specimen is under hydrostatic condition.

The test methods of shear strength of saw-cut surfaces under constant σ_p are identical to those of the tension-induced fractures. The σ_p values are maintained constant at 1, 2 and 3 MPa, and the lateral stress σ_o varies from 2 to 10 MPa. The direct shear test methods follow the ASTM (D5607) standard practice. The constant normal stresses on the fracture are varied form 1, 2, 3 and 4 MPa

1.3.4 Development of mathematical relations

Results from laboratory measurements in terms of major principal stresses (σ_1) corresponding to the peak shear strength as a function of lateral stress (σ_o) and peak shear strength (τ) as a function of normal stress (σ_n) for various σ_p/σ_o ratios. The testing results have been used to develop relations between friction angle (ϕ) and σ_p/σ_o ratios, cohesion (c) and σ_p for determine a new failure criterion for joint shear strength under true triaxial stress.

1.3.5 Conclusions and thesis writing

All research activities, methods, and results are documented and complied in the thesis. The research findings are published in the conference proceedings or journals.

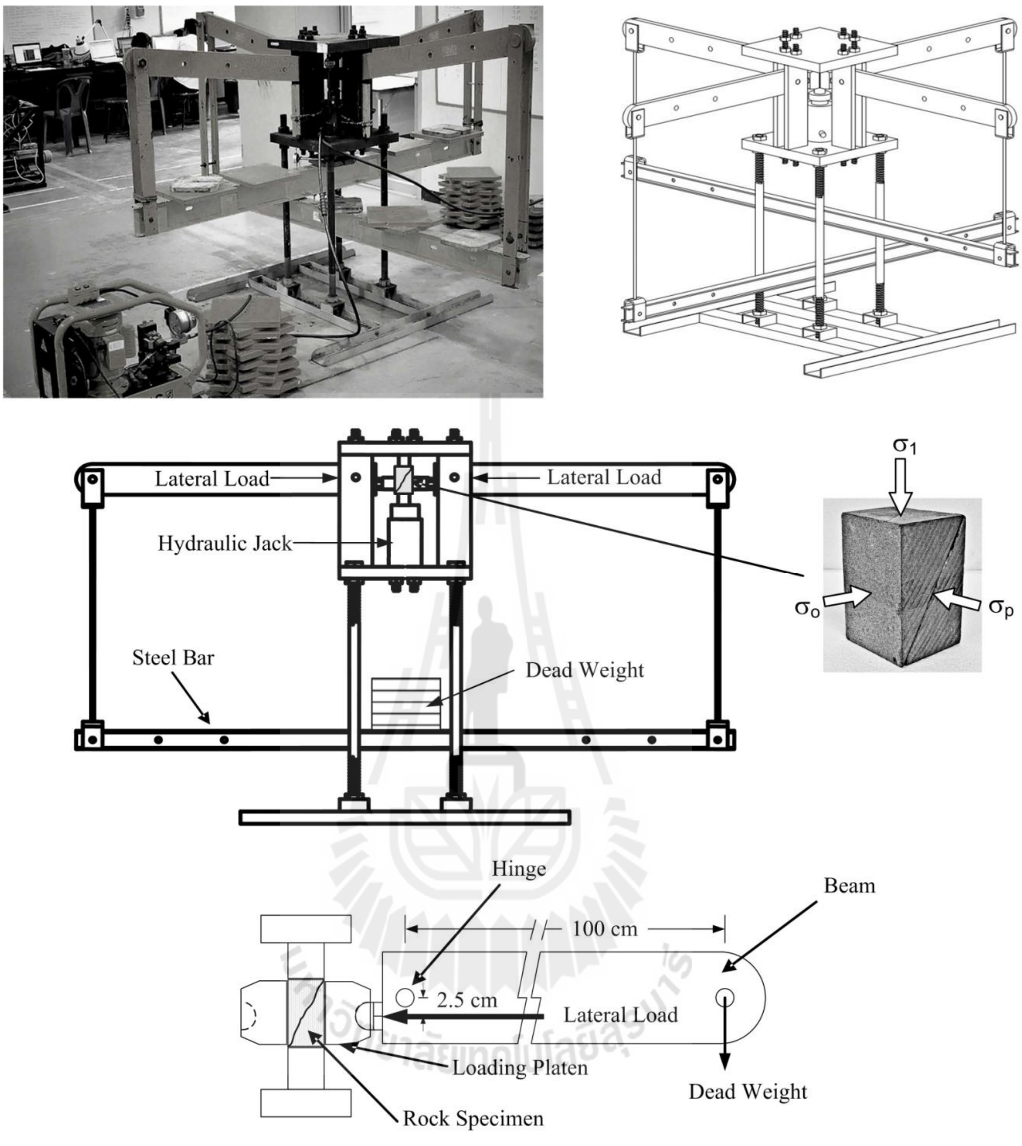

Figure 1.2 Polyaxial load frame used in this study.

1.4 Scope and limitations

The scope and limitations of the research include as follows.

1. Laboratory experiments are conducted on specimens prepare from Phu Kradung, Phra Wihan, and Phu Phan formations.
2. The true triaxial shear tests have been made under constants lateral stresses and direct shear tests have been tested with constant normal stress 4 level.
3. Up to 70 samples are tested for each rock type, with the dimensions of $7.6 \times 7.6 \times 12.7$ cm^3 for true triaxial shear test.
4. The direct shear test specimens have dimensions of $10 \times 10 \times 15$ cm^3.
5. All tests are conducted under ambient temperature.
6. All tested fractures are artificially made in the laboratory by tension induced method.
7. All testing are made under dry condition.
8. No field testing will be performed.
9. A new shear strength criterion has been derived from the test results.

1.5 Thesis contents

This first chapter introduces the thesis by briefly describing the rationale and background and identifying the research objectives. The third section identifies the research methodology. The fourth section describes scope and limitations. The fifth section gives a chapter by chapter overview of the contents of this thesis.

The second chapter summarizes results of the literature review. Chapter three describes samples preparation. The laboratory tests are described in chapter four. The results of all tested and development of mathematical relations are presented in chapter five. Chapter six provides the conclusion and recommendations for future research studies.

CHAPTER II

LITERATURE REVIEW

2.1 Introduction

The topics reviewed here include factors affecting to joint shear strength, true triaxial or polyaxial stress in previous research and testing device development.

2.2 Factors affecting to joint shear strength

Ramamurthy and Arora (1994) state that most of the rational approaches to the design of structures on or in a rock mass are based on the strength response of the rock mass. Realizing this important aspect, the present investigation was undertaken to understand the strength response of jointed rocks. The objective was achieved by simulating joints in intact isotropic rock cores in the laboratory.

Three materials, namely, plaster of Paris, Jamrani sandstone and Agra sandstone were selected. The intact specimens of these materials provided a wide range of compressive strength. A special technique was devised to develop joints varying in number and inclination. Based on this extensive experimentation, a joint factor J_f, has been evolved to account for the number of joints per metre length, inclination of the sliding joint and the shear strength along this joint. This factor is found to be uniquely related to the ratio of compressive strength of jointed rock to that of the intact rock irrespective of the type of rock. A strength criterion for jointed rocks is proposed and the parameters defining this criterion can be evolved simply by knowing the joint factor, compressive strength of intact rock and triaxial strength of intact specimens at two convenient confining pressures. The empirical relations developed have been verified with similar data for other jointed rocks and model materials.

Kusumi et al. (1997) state that a new formulation of shear strength for irregular rock joints by Ladanyi's shear strength criterion (1970) is only applied to the regular triangular joints. The purpose of this study is the proposal of a new shear strength criterion which is applied to irregular joints. First of all, the appropriate estimation method of irregular joint profiles must be quantitatively estimated. The artificial plaster specimens which have four different JRC profiles, and the sandstone specimens including the irregular joint are applied on the direct shear test. The measurement and analysis of joint surface profile for each specimen using laser profilometer have conducted. As the results, the new experimental equations which exactly represent the shear strength parameters included in Ladanyi's shear strength criterion was proposed, and it is recognized that this new experimental equations can be applied for the rock specimens having the irregular joint.

Zhao (1997) states that the JRC-JCS model (Barton's JRC-JCS shear strength criterion 1976) tends to over-predict the shear strength for those natural joints with less matched surfaces. To overcome this shortcoming, a new JRC-JMC shear strength criterion is proposed in order to include the effects of both joint surface roughness and joint matching, in the form of $\tau = \sigma_n \cdot \tan [JRC \cdot JMC \cdot \log_{10} (JCS/\sigma_n) + \phi_r]$. The new JRC-JMC model provides appropriate fining of the shear test results and gives a better interpretation and prediction, particularly for natural joints that do not have perfectly matched surfaces.

Grasselli and Egger (2002) propose a new constitutive criterion, relating stress and displacements, is proposed to model the shear resistance of joints under constant normal load conditions. It is based on an empirical description of the surface, and on the results from more than 50 constant normal-load direct-shear tests performed on replicas of tensile joints and on induced tensile fractures for seven rock types. This constitutive model is able to describe experimental shear tests conducted in the laboratory. Moreover, the parameters required in the model can be easily measured through standard laboratory tests. The proposed criterion was also used to estimate the joint roughness coefficient (JRC) value. The predicting values were successfully correlated with JRC values obtained by back analysis of shear tests.

Maksimovic (1996) proposes a non -linear failure envelope of hyperbolic type in terms of effective stresses for rock discontinuities is described by a simple three parameter expression, which contains the basic angle of friction, the roughness angle and the median angle pressure. The components of friction, dilation and breakage of asperities are derived. The proposed expressions are related to the widely used, failure law, of a logarithmic type proposed by Barton and the simple correspondence of ‘two sets of parameters derived. Comparison with the power type expressions and possibilities for conversion is presented. Several experimental results are used for verification of the proposed relations. It is shown that the proposed hyperbolic relation has significant advantages.

Yang et al. (2001) state that the Fourier series function is applied to resolve the original JRC profile. Then, two model joints that consist of the first five and forty harmonics are tested to investigate the role of primary and secondary asperity in the shear behavior. From the experimental observation, at very low stress levels the secondary asperity has a remarkable effect on the joint strength, but not on the dilation. The dilation behavior is mainly controlled by the large-scale primary asperity. A single roughness parameter, such as the JRC or D; is not enough to describe the roughness behavior contributed by the numerous scaled asperities. This study found that the fractal parameter, D or H; is better used to reflect the roughness property for the rougher profiles than smoother ones. In fact, the H (or D) is represented for the frequency of asperity appearance than the asperity size. Thus, the fractal parameter (D or H) better reflects the roughness property contributed by the secondary asperity. In contrast, the JRC produces a good response to the roughness property in the asperity size or slope angle. To capture the actual roughness characteristics of a natural joint surface, contributed by both the primary and secondary asperities, combining the JRC and H (or D) has a positive benefit.

Fardin et al. (2001) state that accurate determination of surface roughness of rock joints at the large-scale is essential for proper rock mass characterization. Surface roughness of rock joints is commonly characterized using small samples. However, since roughness parameters of rock joints are scale-dependent and their descriptors change with scale, a systematic investigation has been carried out to understand the effect of scale on the surface roughness of rock joints. The fractal parameters, i.e. the fractal dimension *D* and amplitude parameter *A* describing surface roughness of the replica, were calculated on the basis of the Roughness–Length Method. To investigate the scale-dependency of surface roughness of rock joints, ten sampling windows ranging in size from 100 mm×100 mm to 1000 mm×1000 mm were selected from the central part of the replica and their fractal parameters were calculated. The results show that both *D* and *A* are scale-dependent and their values decrease with increasing size of the sampling windows. This scale-dependency is limited to a certain size, defined as the stationarity threshold, and for sampling windows larger than the stationarity threshold the estimated parameters remain almost constant. It is concluded that, for surface roughness to be accurately characterized on a laboratory scale or in the field, samples need to be equal to or larger than the stationarity limit.

Babanouri et al. (2011) state that although many researchers have studied normal and shear behavior of fractures under stresses, the over-consolidation effect on the slip/shear behavior of discontinuities has not been considered. The over-consolidation behavior of non-planar rock fractures should be considered when deposition-consolidation-erosion (or excavation) sequences occur. Plaster replicas of representative natural rock joint surfaces were prepared for this study. In this case, the surface roughness and other geometrical properties remain constant during the laboratory direct shear tests. It was observed that the shear strength within a large range of roughness, joint wall strength and normal stress values significantly increases with increasing over-consolidation ratio. According to the test results, a new model is developed as an extended form of Barton's shear failure criterion for rock joints. This model considers the effect of various paths of normal loading/unloading before shearing and over-consolidation ratio (OCR) in a fracture. A new joint over-closure (JOC) parameter is also introduced as the ratio of closure in over-closed to normally closed conditions.

2.3 True triaxial or polyaxial stress in previous research

Singh et al. (1988) studied the effect of intermediate principal stress on strength of anisotropic rock mass. The Mohr-Coulomb criterion needs to be modified for highly anisotropic rock material and jointed rock masses. Taking σ_2 into account, a new strength criterion is suggested because both a σ_2 and a σ_3 would contribute to the normal stress on the existing plane of weakness. This criterion explains the enhancement of strength (σ_2-σ_3) in the underground openings because σ_2 along the tunnel axis is not relaxed significantly. Another cause of strength enhancement is less reduction in the mass modulus in tunnels due to constrained dilatancy. Empirical correlations obtained from data from block shear tests and uniaxial jacking tests have been suggested to estimate new strength parameters. A correlation for the tensile strength of the rock mass is presented. Finally, Hock and Brown theory is extended to account for σ_2. A common strength criterion for both supported underground openings and rock slopes is suggested.

Alexeev et al. (2008) studied the effect of stress state factor on fracture of sandstones under true triaxial loading. Experimental results concerning rocks deformation and fracture under true triaxial compression have revealed a misfit between strain state and stress state, strain state varying from generalized compression to generalized shear at $\sigma_3 \neq 0$. This misfit can lead to data misinterpretation during stress field reconstruction after unloading. The fracture of rock specimens under true triaxial compression occurs by a combined longitudinal/transverse shear and produces the highest dilatancy. An increase in the hydrostatic pressure level diminishes limiting values of shear strains and suppresses the dilatancy effect. A maximum of dilatancy coincides with a maximum of fresh surface area formed during the fracture of the rock. Generalized cleavage of rocks becomes energetically disadvantageous in a true triaxial compressive stress field. Failure occurs through longitudinal/transverse shear cracking. The embrittlement effect found experimentally is inconsistent with the conclusion of Haimson and Chang (2000), who found an additive effect of minimal compressive stress σ_3 and intermediate compressive stress σ_2 on strength of rocks. This discrepancy is obviously caused by the high initial porosity and dilatancy of some sandstone, as seen in the data comparison in Figure 2.1.

2.4 Testing device development

Rao and Tiwari (2008) poposed a polyaxial loading system (Figures 2.2 and 2.3) that was designed and developed at Indian Institute of Technology Delhi, India for laboratory testing of mechanical behavior of rock mass. The large-scale rock mass models of different joint geometry can be tested under polyaxial stress state simulating in situ stress conditions using this true-triaxial system. The system consists of a 1000 kN capacity vertical frame, a biaxial frame of 300 kN capacity fitted with two pairs of hydraulic jacks and platens, constant confining pressure unit for applying, monitoring, and maintaining horizontal stresses (σ_2 and σ_3) on specimen faces, eight-channel data acquisition system, and a personal computer to record all load and deformation data. Its working was verified by conducting true triaxial testing on several models specimens of sand-lime blocks having three sets of orthogonal joints.

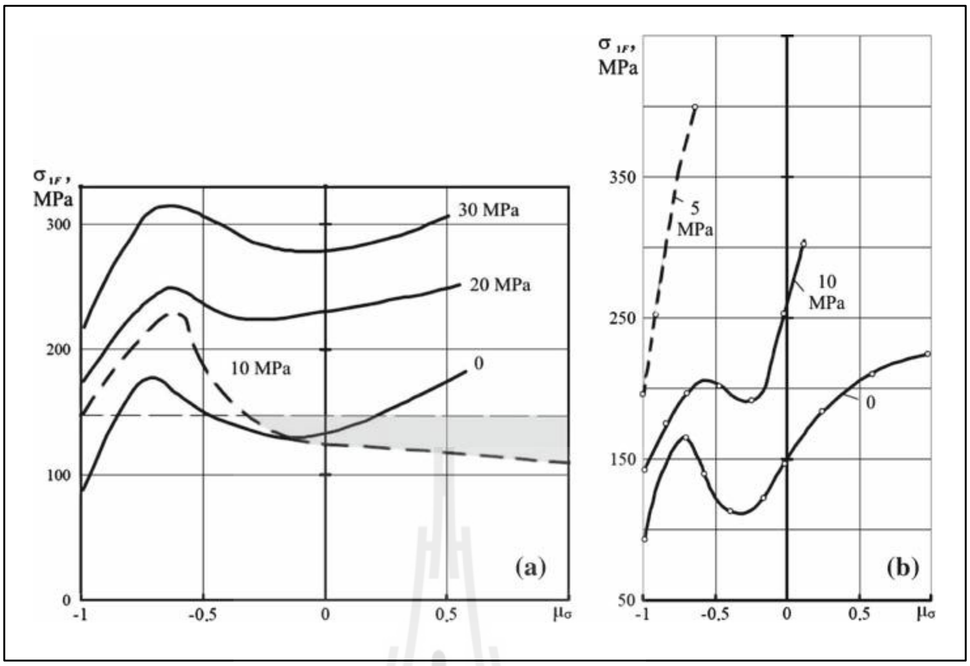

Figure 2.1 Stress state factor dependence of strength for sandstones: (a) Highly porous sandstone from A.A. Skotchinsky mine. (b) Less porous sandstones of A.F.Zasyadko mine (solid lines) and Yunkom mine (dash line). Figures near curves show values σ_3. Filled area in Figure 1a indicates condition of embrittlement (Alexeev et al, 2008).

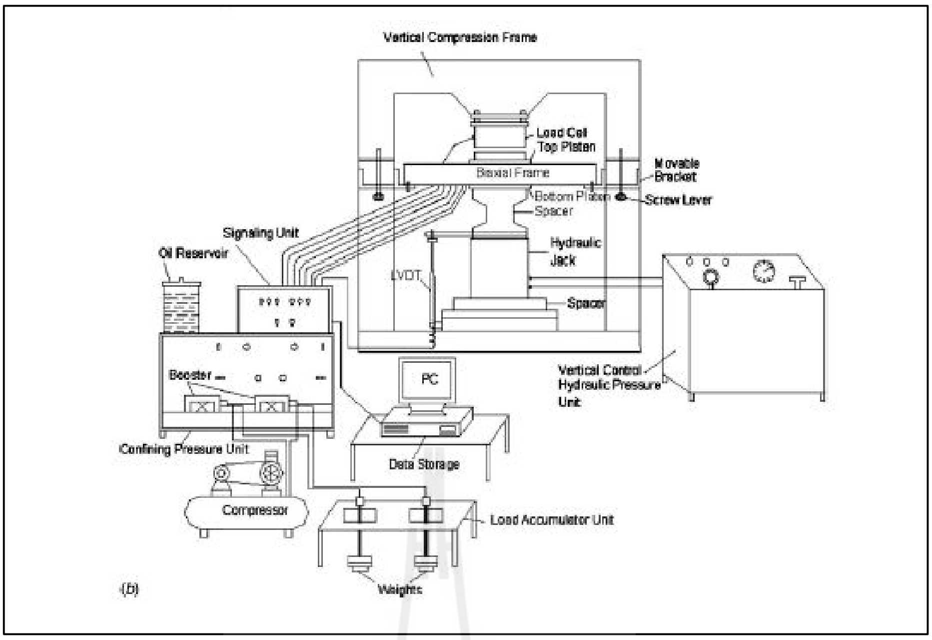

Figure 2.2 Schematic diagram for setup of true triaxial system (Rao and Tiwari, 2008).

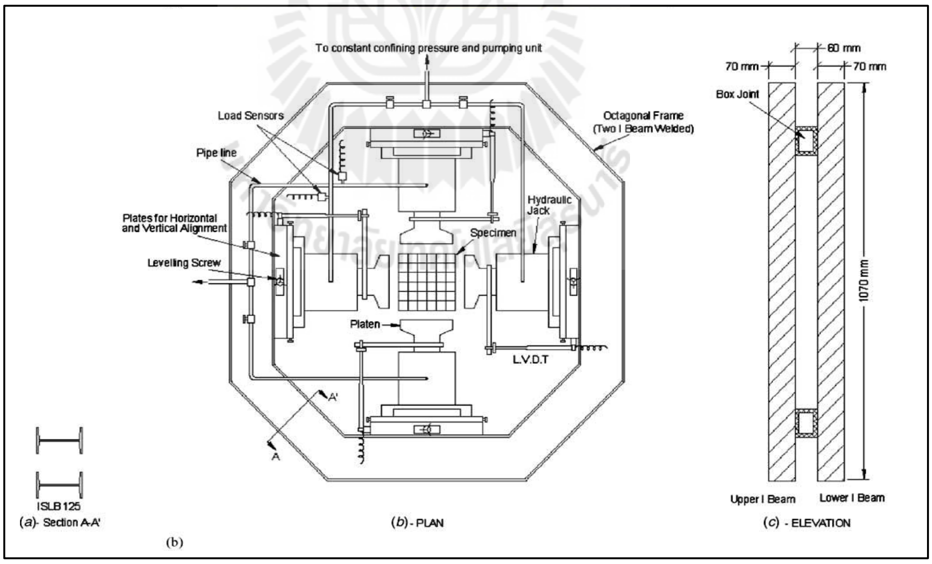

Figure 2.3 Sketch of biaxial frame with accessories (Rao and Tiwari, 2008).

CHAPTER III

SAMPLE PREPARATION

3.1 Introduction

This chapter describes the sample preparation for the direct shear tests and the shear tests under true triaxial stress state.

3.2 Sample preparation

The specimens used for the true triaxial shear tests are prepared from the Phu Kradung, Phu Phan and Phra Wihan sandstones (hereafter designated as PKSS, PPSS and PWSS, shows in Figure 3.1). They are cut to obtain rectangular blocks with nominal dimensions of 76×76×126 mm^3. These rocks are classified as fine-grained quartz sandstones with highly uniform texture and density. A line load is applied to obtain a tension-induced fracture diagonally across the sandstone block, as shown in Figure 3.2. The normal to the fracture plane makes an angle of 59.1° with the major axis of the specimen. All fractures are clean and well mated. The asperity amplitudes on the fracture planes are measured from the laser-scanned profiles along the shear direction. The readings are made to the nearest 0.01 mm. The maximum amplitudes are used to estimate the joint roughness coefficients (JRC) of each fracture based on Barton's chart (Barton, 1982). The joint roughness coefficients are averaged as 8, 6 and 6 for PKSS, PPSS and PWSS, respectively. Figure 3.3 shows examples of the laser scanned profiles for the three sandstones. Some three-dimensional image profiles are shown in Figure 3.4.

For the specimens with the saw-cut surface, two sandstone blocks are used to form a complete pair of specimens primarily to avoid the effect of the groove caused by the cutting blade (Figure 3.5). Each block is cut diagonally and hence obtaining the smooth fractures with the normal making an angle of 59.1° with the major axis of the specimen. All specimens are oven-dried before testing.

For the direct shear test specimens a line load is applied to obtain a tension-induced fracture at the mid-section of the 100×100×160 mm^3 sandstone blocks (Figure 3.6). The fracture area is 100×100 mm^2. Table 3.1 - 3.4 shows physical properties of specimen for all conditions.

Table 3.1 Sandstone specimens prepared for true triaxial shear tests.

Specimen No.	**Dimension (cm^3)**	**Density (g/cc)**
PKSS-01	7.61×7.60×12.70	2.55
PKSS-02	7.60×7.60×12.72	2.53
PKSS-03	7.62×7.63×12.63	2.50
PKSS-04	7.61×7.62×12.62	2.55
PKSS-05	7.62×7.60×12.63	2.53
PKSS-06	7.63×7.60×12.61	2.54
PKSS-07	7.60×7.61×12.62	2.56
PKSS-08	7.63×7.61×12.60	2.52
PKSS-09	7.63×7.62×12.63	2.54
PKSS-10	7.60×7.65×12.70	2.53
PKSS-11	7.62×7.64×12.64	2.52
PKSS-12	7.63×7.63×12.60	2.53
PKSS-13	7.60×7.60×12.65	2.56
PKSS-14	7.60×7.61×12.62	2.57
PKSS-15	7.62×7.61×12.64	2.52
PKSS-16	7.60×7.61×12.62	2.54
PKSS-17	7.60×7.60×12.62	2.54
PKSS-18	7.62×7.61×12.67	2.53
PKSS-19	7.60×7.61×12.62	2.54
PKSS-20	7.60×7.63×12.63	2.56
PKSS-21	7.61×7.61×12.70	2.56
PKSS-22	7.62×7.60×12.64	2.54
PKSS-23	7.62×7.64×12.60	2.53
PKSS-24	7.60×7.61×12.64	2.54
PKSS-25	7.60×7.61×12.62	2.51
PKSS-26	7.60×7.62×12.63	2.54
PKSS-27	7.60×7.61×12.63	2.53
PKSS-28	7.63×7.62×12.62	2.55
PKSS-29	7.62×7.63×12.62	2.5
PKSS-30	7.60×7.61×12.62	2.56
PKSS-31	7.60×7.60×12.60	2.53
PKSS-32	7.60×7.61×12.71	2.55

Table 3.1 Sandstone specimens prepared for true triaxial shear tests (continue).

Specimen No.	**Dimension (cm^3)**	**Density (g/cc)**
PPSS-01	7.63×7.63×12.70	2.45
PPSS-02	7.65×7.62×12.63	2.42
PPSS-03	7.65×7.63×12.63	2.43
PPSS-04	7.64×7.62×12.66	2.43
PPSS-05	7.60×7.60×12.60	2.39
PPSS-06	7.60×7.65×12.60	2.36
PPSS-07	7.60×7.61×12.62	2.44
PPSS-08	7.63×7.61×12.64	2.46
PPSS-09	7.60×7.61×12.62	2.40
PPSS-10	7.62×7.62×12.60	2.46
PPSS-11	7.63×7.60×12.67	2.45
PPSS-12	7.60×7.61×12.62	2.42
PPSS-13	7.62×7.61×12.60	2.39
PPSS-14	7.62×7.60×12.60	2.38
PPSS-15	7.63×7.65×12.70	2.40
PPSS-16	7.62×7.60×12.70	2.44
PPSS-17	7.60×7.61×12.62	2.41
PPSS-18	7.62×7.62×12.60	2.42
PPSS-19	7.63×7.60×12.67	2.47
PPSS-20	7.60×7.61×12.62	2.46
PPSS-21	7.62×7.61×12.60	2.39
PPSS-22	7.62×7.63×12.63	2.45
PPSS-23	7.63×7.64×12.66	2.43
PPSS-24	7.61×7.60×12.60	2.43
PPSS-25	7.61×7.63×12.71	2.42
PPSS-26	7.62×7.62×12.65	2.45
PPSS-27	7.63×7.62×12.70	2.43
PPSS-28	7.60×7.61×12.60	2.39
PPSS-29	7.63×7.63×12.62	2.42
PPSS-30	7.65×7.62×12.66	2.40
PPSS-31	7.60×7.60×12.63	2.43
PPSS-32	7.62×7.62×12.61	2.38

Table 3.1 Sandstone specimens prepared for true triaxial shear tests (continue).

Specimen No.	Dimension (cm^3)	Density (g/cc)
PWSS-01	7.60×7.60×12.64	2.21
PWSS-02	7.63×7.62×12.60	2.23
PWSS-03	7.62×7.65×12.65	2.23
PWSS-04	7.63×7.62×12.67	2.19
PWSS-05	7.64×7.62×12.64	2.24
PWSS-06	7.62×7.62×12.65	2.26
PWSS-07	7.63×7.67×12.63	2.22
PWSS-08	7.60×7.61×12.60	2.23
PWSS-09	7.62×7.61×12.60	2.23
PWSS-10	7.62×7.60×12.60	2.24
PWSS-11	7.63×7.65×12.70	2.26
PWSS-12	7.62×7.60×12.70	2.19
PWSS-13	7.60×7.63×12.62	2.22
PWSS-14	7.62×7.60×12.60	2.26
PWSS-15	7.63×7.60×12.60	2.26
PWSS-16	7.60×7.63×12.62	2.29
PWSS-17	7.62×7.62×12.62	2.25
PWSS-18	7.62×7.60×12.63	2.23
PWSS-19	7.63×7.62×12.63	2.26
PWSS-20	7.61×7.60×12.60	2.23
PWSS-21	7.61×7.60×12.60	2.22
PWSS-22	7.60×7.60×12.62	2.20
PWSS-23	7.62×7.63×12.63	2.25
PWSS-24	7.60×7.60×12.62	2.17
PWSS-25	7.62×7.64×12.63	2.28
PWSS-26	7.63×7.63×12.61	2.30
PWSS-27	7.60×7.61×12.62	2.30
PWSS-28	7.63×7.63×12.62	2.26
PWSS-29	7.63×7.63×12.65	2.24
PWSS-30	7.63×7.62×12.70	2.33
PWSS-31	7.60×7.60×12.60	2.30
PWSS-32	7.60×7.60×12.60	2.25

Table 3.2 Sandstone specimens prepared for true triaxial shear tests of tension-induced fractures under constant σ_p.

Specimen No.	Dimension (cm^3)	Density (g/cc)
PKSS-01	7.62×7.60×12.62	2.52
PKSS-02	7.59×7.61×12.58	2.53
PKSS-03	7.63×7.60×12.60	2.52
PKSS-04	7.59×7.58×12.61	2.50
PKSS-05	7.58×7.58×12.61	2.54
PKSS-06	7.60×7.60×12.60	2.50
PKSS-07	7.62×7.61×12.60	2.56
PKSS-08	7.60×7.62×12.63	2.55
PKSS-09	7.59×7.59×12.59	2.54
PKSS-10	7.57×7.59×12.58	2.53
PKSS-11	7.61×7.60×12.60	2.52
PKSS-12	7.62×7.61×12.62	2.53
PKSS-13	7.62×7.59×12.61	2.56
PKSS-14	7.59×7.60×12.59	2.57
PKSS-15	7.57×7.61×12.59	2.51
PKSS-16	7.60×7.61×12.62	2.53
PKSS-17	7.62×7.59×12.60	2.54
PKSS-18	7.60×7.59×12.60	2.53
PKSS-19	7.59×7.62×12.61	2.54
PKSS-20	7.61×7.63×12.58	2.52
PKSS-21	7.58×7.61×12.59	2.56
PKSS-22	7.59×7.60×12.60	2.58
PKSS-23	7.60×7.60×12.62	2.57
PKSS-24	7.61×7.59×12.61	2.56
PKSS-25	7.61×7.58×12.58	2.52
PKSS-26	7.62×7.60×12.59	2.54
PKSS-27	7.60×7.62×12.60	2.53
PKSS-28	7.60×7.61×12.61	2.55

.

Table 3.2 Sandstone specimens prepared for true triaxial shear tests of tension-induced fractures under constant σ_p (continue).

Specimen No.	Dimension (cm^3)	Density (g/cc)
PPSS-01	7.62×7.61×12.60	2.39
PPSS-02	7.62×7.59×12.61	2.42
PPSS-03	7.59×7.60×12.59	2.41
PPSS-04	7.57×7.61×12.60	2.46
PPSS-05	7.58×7.58×12.61	2.38
PPSS-06	7.60×7.60×12.60	2.36
PPSS-07	7.62×7.60×12.60	2.39
PPSS-08	7.60×7.62×12.62	2.42
PPSS-09	7.61×7.61×12.61	2.44
PPSS-10	7.62×7.62×12.62	2.46
PPSS-11	7.61×7.59×12.59	2.45
PPSS-12	7.59×7.61×12.59	2.44
PPSS-13	7.61×7.60×12.61	2.39
PPSS-14	7.60×7.60×12.60	2.38
PPSS-15	7.58×7.62×12.59	2.42
PPSS-16	7.61×7.59×12.62	2.43
PPSS-17	7.60×7.58×12.61	2.41
PPSS-18	7.62×7.60×12.59	2.42
PPSS-19	7.60×7.60×12.62	2.49
PPSS-20	7.59×7.62×12.59	2.45
PPSS-21	7.60×7.61×12.60	2.39
PPSS-22	7.58×7.60×12.60	2.46
PPSS-23	7.61×7.61×12.61	2.43
PPSS-24	7.62×7.60×12.63	2.44
PPSS-25	7.60×7.60×12.59	2.46
PPSS-26	7.62×7.58×12.60	2.45
PPSS-27	7.61×7.60×12.62	2.43
PPSS-28	7.60×7.59×12.60	2.39

Table 3.2 Sandstone specimens prepared for true triaxial shear tests of tension-induced fractures under constant σ_p (continue).

Specimen No.	**Dimension (cm^3)**	**Density (g/cc)**
PWSS-01	7.59×7.60×12.62	2.20
PWSS-02	7.61×7.58×12.59	2.22
PWSS-03	7.58×7.62×12.60	2.23
PWSS-04	7.59×7.61×12.62	2.19
PWSS-05	7.60×7.59×12.61	2.25
PWSS-06	7.61×7.62×12.61	2.26
PWSS-07	7.62×7.61×12.59	2.20
PWSS-08	7.60×7.59×12.58	2.23
PWSS-09	7.60×7.58×12.60	2.24
PWSS-10	7.61×7.60×12.61	2.25
PWSS-11	7.59×7.60×12.60	2.26
PWSS-12	7.58×7.62×12.59	2.19
PWSS-13	7.60×7.62×12.62	2.22
PWSS-14	7.61×7.61×12.59	2.26
PWSS-15	7.60×7.62×12.59	2.28
PWSS-16	7.59×7.59×12.58	2.29
PWSS-17	7.59×7.59×12.60	2.25
PWSS-18	7.61×7.62×12.58	2.23
PWSS-19	7.62×7.61×12.60	2.26
PWSS-20	7.60×7.63×12.61	2.24
PWSS-21	7.58×7.62×12.62	2.26
PWSS-22	7.59×7.59×12.58	2.22
PWSS-23	7.60×7.58×12.59	2.21
PWSS-24	7.62×7.58×12.61	2.19
PWSS-25	7.61×7.62×12.60	2.26
PWSS-26	7.60×7.58×12.61	2.28
PWSS-27	7.59×7.61×12.62	2.25
PWSS-28	7.58×7.60×12.61	2.23

Table 3.3 Sandstone specimens prepared for true triaxial shear tests of smooth surfaces.

Specimen No.	Dimension (cm^3)	Density (g/cc)
PKSS-01	7.60×7.61×12.60	2.51
PKSS-02	7.62×7.60×12.59	2.52
PKSS-03	7.61×7.62×12.61	2.49
PKSS-04	7.60×7.59×12.62	2.54
PKSS-05	7.58×7.60×12.60	2.53
PKSS-06	7.63×7.61×12.60	2.51
PKSS-07	7.59×7.62×12.59	2.56
PKSS-08	7.60×7.59×12.58	2.52
PKSS-09	7.61×7.59×12.59	2.52
PKSS-10	7.62×7.60×12.60	2.51
PKSS-11	7.60×7.61×12.62	2.49
PKSS-12	7.60×7.62×12.61	2.56
PPSS-01	7.61×7.60×12.60	2.38
PPSS-02	7.61×7.61×12.59	2.40
PPSS -03	7.59×7.61×12.61	2.45
PPSS -04	7.58×7.59×12.61	2.43
PPSS -05	7.59×7.61×12.60	2.40
PPSS -06	7.61×7.62×12.60	2.39
PPSS -07	7.60×7.60×12.62	2.38
PPSS -08	7.60×7.59×12.59	2.47
PPSS -09	7.59×7.61×12.58	2.46
PPSS -10	7.58×7.62×12.60	2.44
PPSS -11	7.62×7.60×12.60	2.40
PPSS -12	7.61×7.61×12.61	2.42
PWSS-01	7.60×7.61×12.62	2.24
PWSS -02	7.59×7.59×12.59	2.25
PWSS -03	7.61×7.58×12.61	2.27
PWSS -04	7.59×7.60×12.62	2.19
PWSS -05	7.60×7.61×12.60	2.28
PWSS -06	7.61×7.59×12.60	2.24
PWSS -07	7.61×7.61×12.61	2.27
PWSS -08	7.60×7.62×12.62	2.23
PWSS -09	7.59×7.58×12.58	2.18
PWSS -10	7.62×7.60×12.60	2.22
PWSS -11	7.61×7.60×12.61	2.25
PWSS -12	7.60×7.61×12.59	2.23

Table 3.4 Sandstone specimens prepared for direct shear tests of tension-induced fractures.

Specimen No.	Dimension (cm^3)	Density (g/cc)
PKSS-01	7.61×7.60×12.60	2.20
PKSS-02	7.62×7.61×12.62	2.23
PKSS-03	7.62×7.59×12.61	2.24
PKSS-04	7.60×7.60×12.61	2.25
PPSS-01	7.63×7.60×12.60	2.38
PPSS-02	7.61×7.61×12.60	2.36
PPSS-03	7.62×7.63×12.61	2.39
PPSS-04	7.63×7.62×12.61	2.42
PWSS-01	7.60×7.60×12.60	2.25
PWSS-02	7.62×7.60×12.62	2.27
PWSS-03	7.62×7.62×12.70	2.19
PWSS-04	7.61×7.64×12.65	2.28

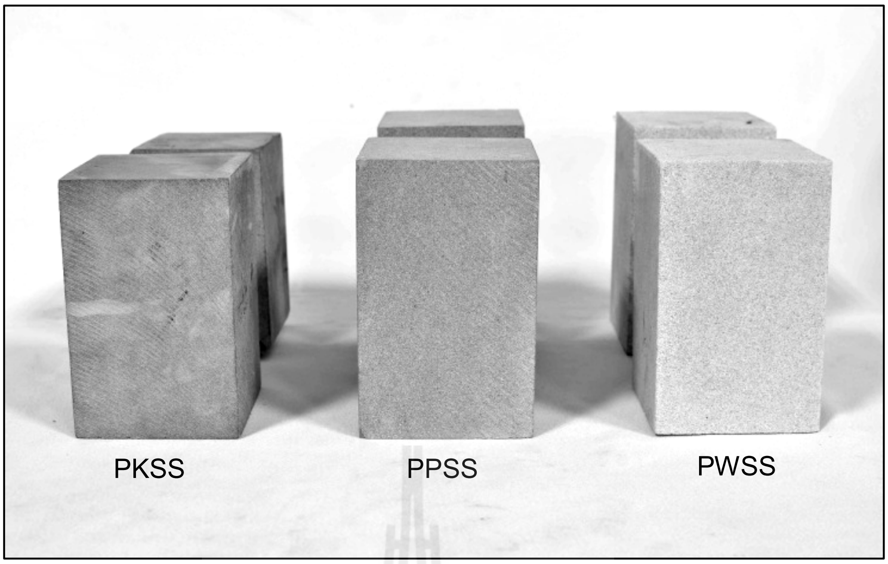

Figure 3.1 Some specimens before tension-induced fracture of the true triaxial shear test.

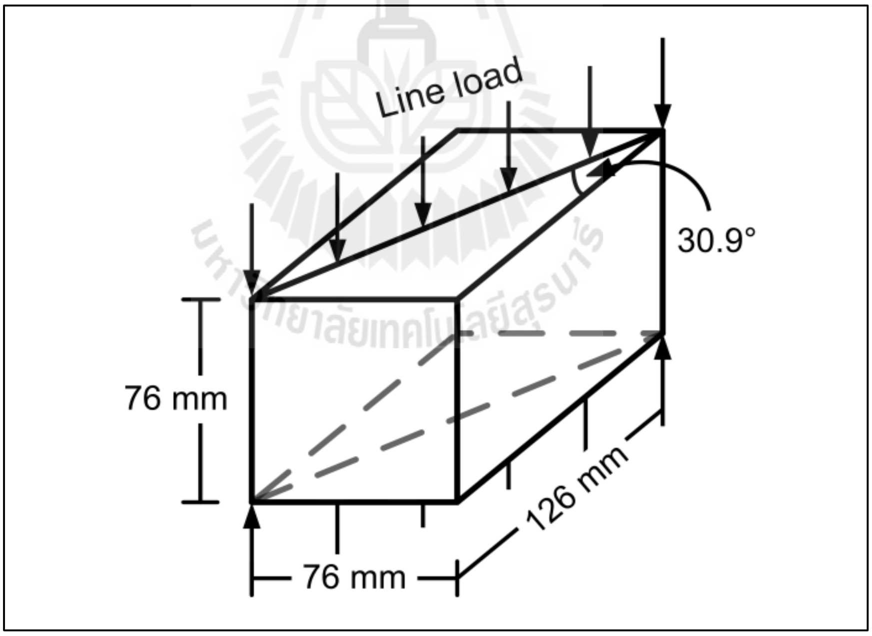

Figure 3.2 Line load applied to obtain tension-induced fracture in sandstone specimen.

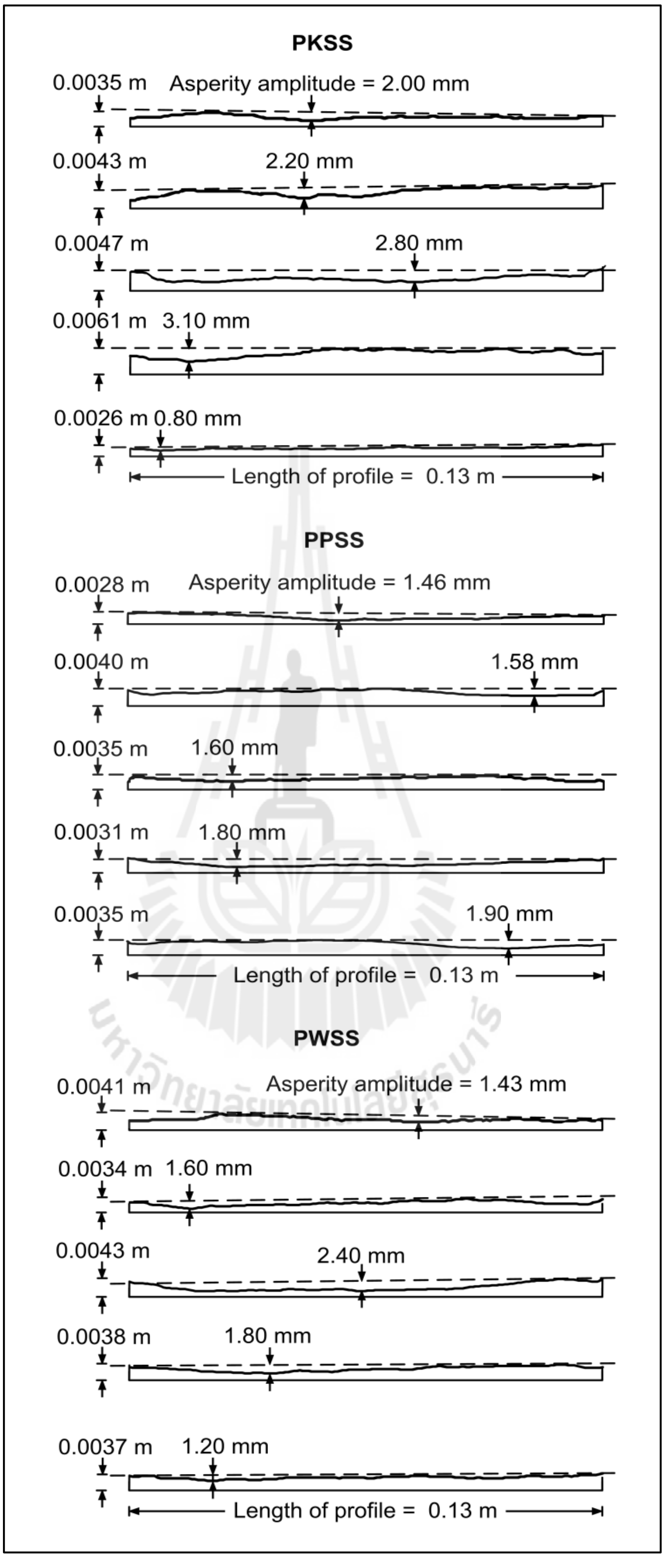

Figure 3.3 Examples of laser-scanned profiles to measure the maximum asperity amplitude to estimate the joint roughness coefficient (JRC).

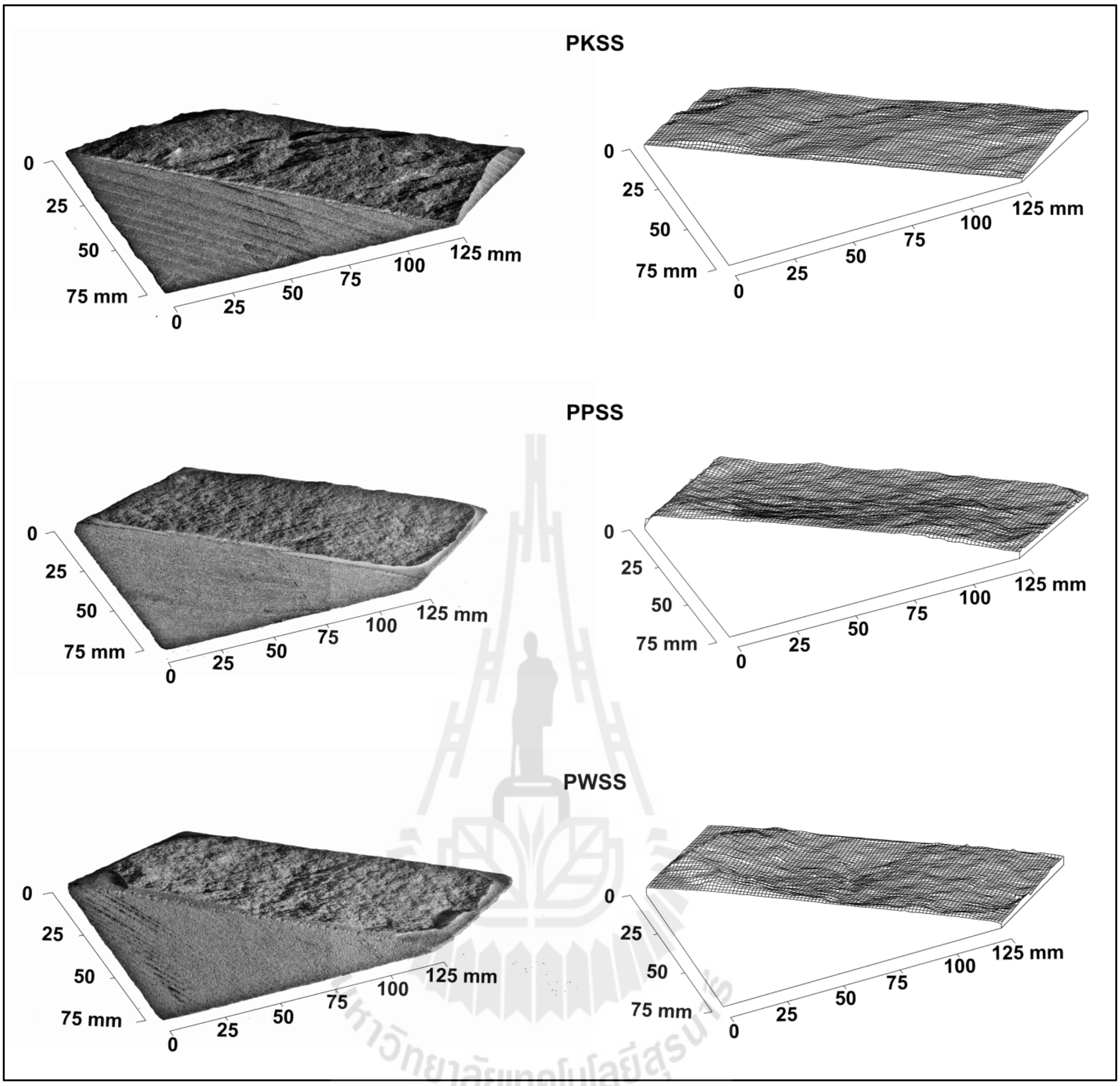

Figure 3.4 Some tension-induced fractures and their laser scanned images.

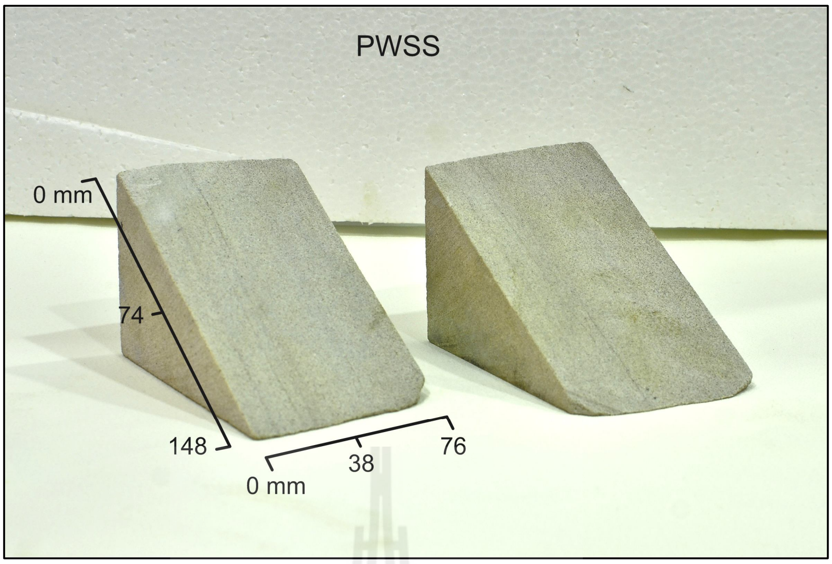

Figure 3.5 Some specimens prepared for shear strength of saw-cut surfaces.

Figure 3.6 Some specimens prepared for direct shear tests.

CHAPTER IV

LABORATORY TESTING

4.1 Introduction

The objective of this section is to experimentally determine the shear resistance of fractures in sandstone specimens under true triaxial stresses. The effort involves performing true triaxial shear tests on tension-induced fractures and smooth saw-cut surfaces by using a polyaxial load frame.

4.2 Polyaxial load frame

A polyaxial load frame (Fuenkajorn and Kenkhunthod, 2010; Fuenkajorn et al., 2012) is used to apply true triaxial stresses to the specimens (Figure 4.1). One of the lateral stresses is parallel to the strike of the fracture plane which is designated as σ_p. The other is normal to the strike of the fracture plane and is designated as σ_o. They are applied by two pairs of 152 cm long cantilever beams set in mutually perpendicular directions. The outer end of each beam is pulled down by a dead weight placed on a lower steel bar linking the two opposite beams underneath. The beam inner end is hinged by a pin mounted between vertical bars on each side of the frame. During testing all beams are arranged nearly horizontally, and hence a lateral compressive load results on the specimen placed at the center of the frame. Using different distances from the pin to the outer weighting point and to the inner loading point, a load magnification of 17 to 1 is obtained. This loading ratio is also used to determine the lateral deformation of the specimen by monitoring the vertical movement of the two steel bars below. Prior to testing the lateral loads are calibrated to obtain the desired lateral stresses using an electronic load cell. The maximum lateral load is designed for 100 kN. The axial stress representing the major principal stress (σ_1) is applied by a 1000-kN hydraulic load cell connected to an electric oil pump via a pressure regulator. Figure 4.2 plots the calibrated curves for use in true triaxial shear test. F is load on the rock sample (kN). W_L is weight on the lower bars (kN).

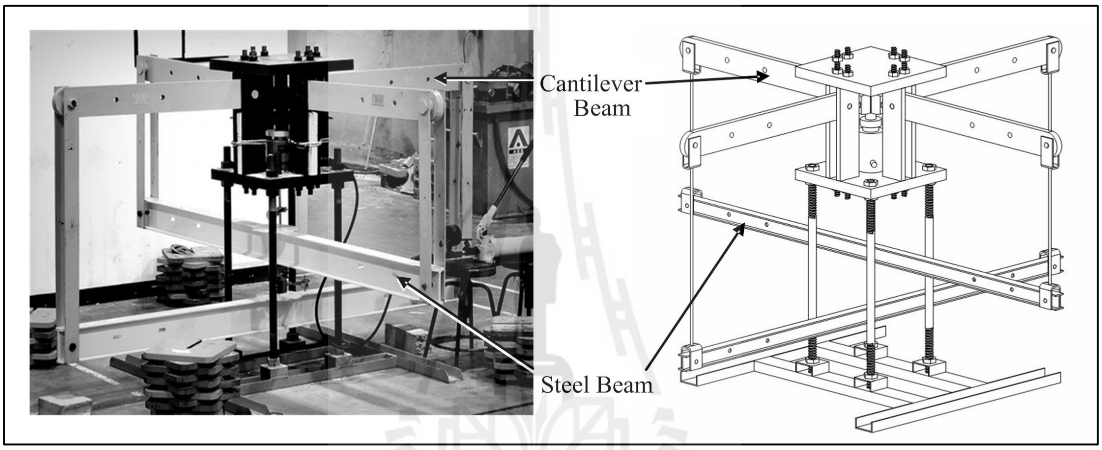

Figure 4.1 The polyaxial load frame for the true triaxial shear test.

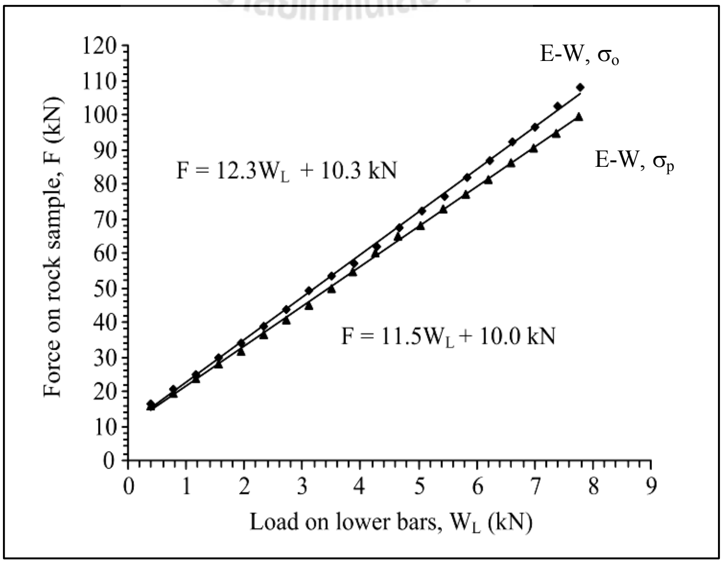

Figure 4.2 Calibrated curves for use in true triaxial shear testing.

4.3 Test procedure

The sandstone specimen is installed into the load frame with neoprene sheets placed at all interfaces between loading platens and rock surfaces to minimize the friction. Dead weights are placed on the two lower bars to obtain the pre-defined magnitude of the lateral stresses (σ_o and σ_p) on the specimen. Simultaneously the axial (vertical) stress is increased to the same value with σ_o to obtain the condition where both shear and normal stresses are zero on the fracture plane. This is set as an initial stress condition. The test is started by increasing the axial stress at a constant rate using the electric oil pump while σ_p and σ_o are maintained constant. The specimen deformations in the three loading directions are monitored. The readings are recorded every 10 kN of the axial load increment until the peak shear stress is reached. Figure 4.3 shows the directions of the applied stresses with respect to the fracture orientation. It is assumed here that the sliding direction is on the σ_1-σ_o plane, i.e., perpendicular to the σ_p axis. As a result the shear stress (τ) and its corresponding normal stress (σ_n) increase with σ_1, which can be determined as follows:

$$\tau = \tfrac{1}{2} (\sigma_1 - \sigma_o) \sin 2\beta \tag{4.1}$$

$$\sigma_n = \tfrac{1}{2} (\sigma_1 + \sigma_o) + \tfrac{1}{2} (\sigma_1 - \sigma_o) \cos 2\beta \tag{4.2}$$

where σ_1 and σ_o are the axial and lateral stresses, and β is the angle between σ_1 and σ_n directions. For all specimens the angle β equals to 59.1°.

The effect of the friction at the interfaces between the steel platen and the lateral neoprene sheet is measured by vertically loading an intact sandstone block with the same dimensions as used above while the constant lateral stresses are applied. A linear relationship between the axial resistance and the applied lateral stresses is obtained as shown in Figure 4.4. The results are used to correct the magnitudes of the axial stress measured during the fracture shearing tests.

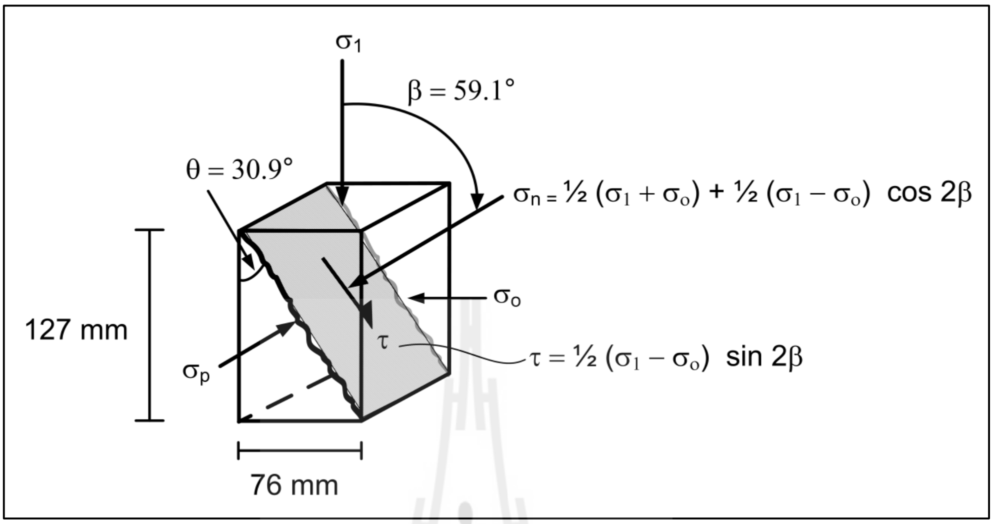

Figure 4.3 Shear (τ) and normal (σ_n) stresses calculated from the applied axial stress (σ_1) and lateral stress on the fracture plane (σ_o).

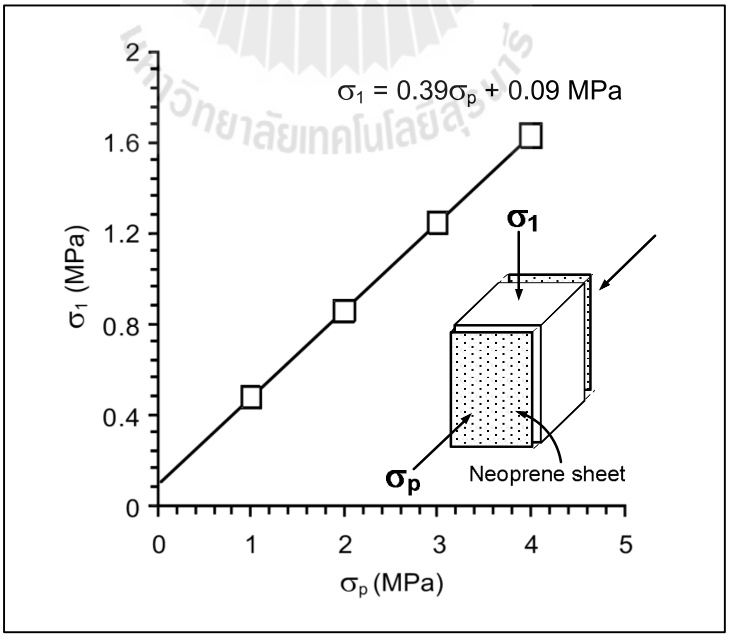

Figure 4.4 Axial resistance between loading platens and neoprene sheets induced by lateral stress (σ_p).

CHAPTER V

TESTING RESULTS

Four test series are performed as follows:

(1) true triaxial shear tests of tension-induced fractures under constant σ_p/σ_o ratio,

(2) true triaxial shear tests of tension-induced fractures under constant σ_p,

(3) true triaxial shear tests of smooth surfaces under constant σ_p, and

(4) direct shear tests of tension-induced fractures.

5.1 Shear strength of tension-induced fractures under constant σ_p/σ_o ratio

For this test series the peak shear strengths are determined for the lateral stress ratios (σ_p/σ_o) of 0, 0.5, 1, 2, 3 and 4. A minimum of four specimens are tested for each lateral stress ratio. The conditions where σ_p/σ_o is 0 and 1 are equivalent to the direct shear testing and the triaxial shear testing. Table 5.1 summarizes the shear strength results for the three sandstone types. Examples of the shear stress-displacement (τ-d_s) curves for some specimens are shown in Figure 5.1. The shear and normal displacements (d_s and d_n) are calculated by:

$$d_s = ½ (d_1 - d_o) \sin 2\beta \qquad (5.1)$$

$$d_n = ½ (d_1 + d_o) + ½ (d_1 - d_o) \cos 2\beta \qquad (5.2)$$

where d_1 and d_o are the specimen displacements monitored in the directions of σ_1 (axial) and σ_o during the test. Figure 5.2 shows the fracture dilation (normal displacement) as a function of the shear displacement monitored during the test.

Table 5.1 Summary of peak shear strengths for σ_p/σ_o = 0, 0.5, 1, 2, 3 and 4.

σ_p/σ_o	σ_p (MPa)	σ_o (MPa)	PKSS			PPSS			PWSS		
			σ_1 (MPa)	σ_n (MPa)	τ (MPa)	σ_1 (MPa)	σ_n (MPa)	τ (MPa)	σ_1 (MPa)	σ_n (MPa)	τ (MPa)
0	0	0.6	14.83	4.16	6.16	21.10	5.72	8.88	20.92	5.68	8.80
	0	1	18.01	5.25	7.37	22.65	6.41	9.37	25.73	7.18	10.71
	0	2	24.21	7.55	9.62	28.01	8.50	11.26	30.79	9.20	12.47
	0	2.5	26.61	8.53	10.44	30.26	9.44	12.01	34.11	10.40	13.69
	0	3	30.26	9.81	11.83	33.56	10.59	13.15	37.67	11.67	15.01
	0	3.5	34.90	11.35	13.59	37.96	12.11	14.92	42.78	13.32	17.00
	0	4	36.43	12.11	14.04	39.49	12.87	15.37	45.60	14.40	18.01
	0	4.5	41.01	13.63	15.81	41.81	13.82	16.16	48.67	15.54	19.13
	0	5	42.54	14.38	16.25	44.07	14.77	16.92	51.05	16.51	19.94
0.5	1	2	17.53	5.88	6.73	20.21	6.55	7.89	24.03	7.51	9.54
	1.5	3	22.00	7.75	8.23	23.42	8.11	8.84	27.15	9.04	10.46
	2	4	27.14	9.79	10.02	27.89	9.97	10.34	33.19	11.29	12.64
	3	6	32.20	12.55	11.35	35.46	13.37	12.76	41.45	14.86	15.35
1	0.6	0.6	7.69	2.37	3.07	11.58	3.34	4.75	13.40	3.80	5.54
	1	1	8.98	3.00	3.46	13.27	4.07	5.31	14.78	4.45	5.97
	2	2	11.92	4.48	4.30	16.12	5.53	6.11	18.41	6.10	7.10
	3	3	15.94	6.24	5.60	18.70	6.93	6.80	21.32	7.57	7.93
	4	4	18.11	7.52	6.11	22.56	8.64	8.04	23.36	8.84	8.38
	5	5	21.72	9.18	7.24	25.22	10.06	8.76	27.69	10.67	9.83
	7	7	25.15	11.54	7.86	30.54	12.88	10.19	31.61	13.15	10.66
2	2	1	7.91	2.73	2.99	12.15	3.79	4.83	13.78	4.20	5.54
	4	2	10.23	4.05	3.56	14.71	5.18	5.55	15.22	5.30	5.72
	6	3	12.38	5.35	4.06	17.32	6.58	6.20	17.98	6.75	6.49
	8	4	14.80	6.70	4.67	19.47	7.87	6.70	20.12	8.03	6.97
	10	5	18.66	8.41	5.91	21.49	9.12	7.14	22.37	9.34	7.52
3	3	1	7.85	2.71	2.97	11.35	3.59	4.48	10.62	3.40	4.16
	6	2	10.02	4.00	3.47	13.12	4.78	4.81	14.23	5.06	5.29
	9	3	11.22	5.06	3.56	14.66	5.91	5.05	15.54	6.13	5.43
	12	4	13.24	6.31	4.00	16.61	7.15	5.46	16.51	7.13	5.45
4	4	1	7.43	2.61	2.79	10.59	3.40	4.15	8.68	2.92	3.33
	8	2	9.03	3.76	3.04	11.82	4.45	4.25	10.73	4.18	3.78
	12	3	10.12	4.78	3.08	13.24	5.56	4.44	12.15	5.29	3.96
	16	4	11.11	5.78	3.08	14.59	6.65	4.58	13.57	6.39	4.15

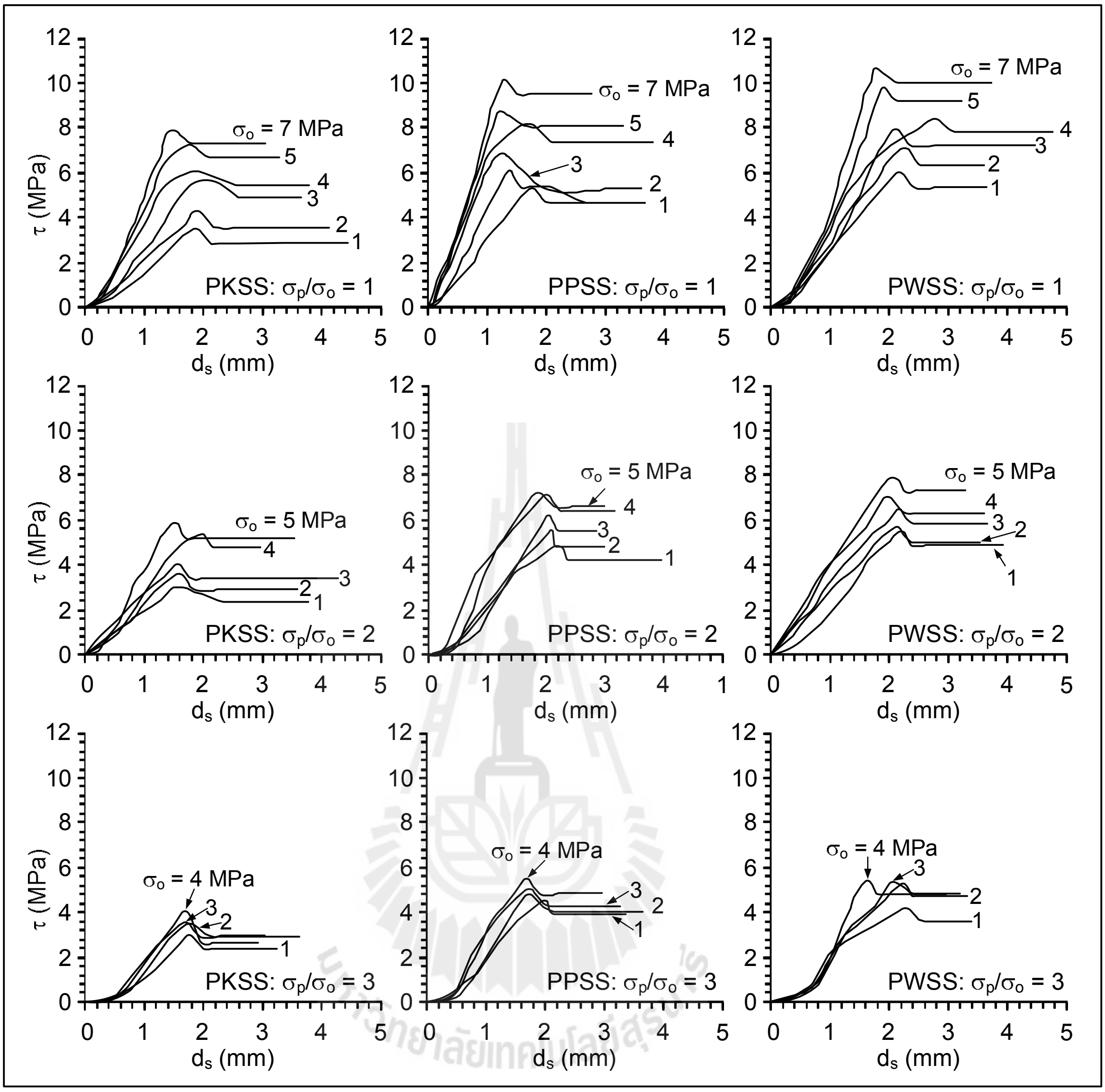

Figure 5.1 Shear stresses (τ) as a function of shear displacement (d_s) for some σ_p/σ_o ratios for (from left to right) PKSS, PPSS and PWSS.

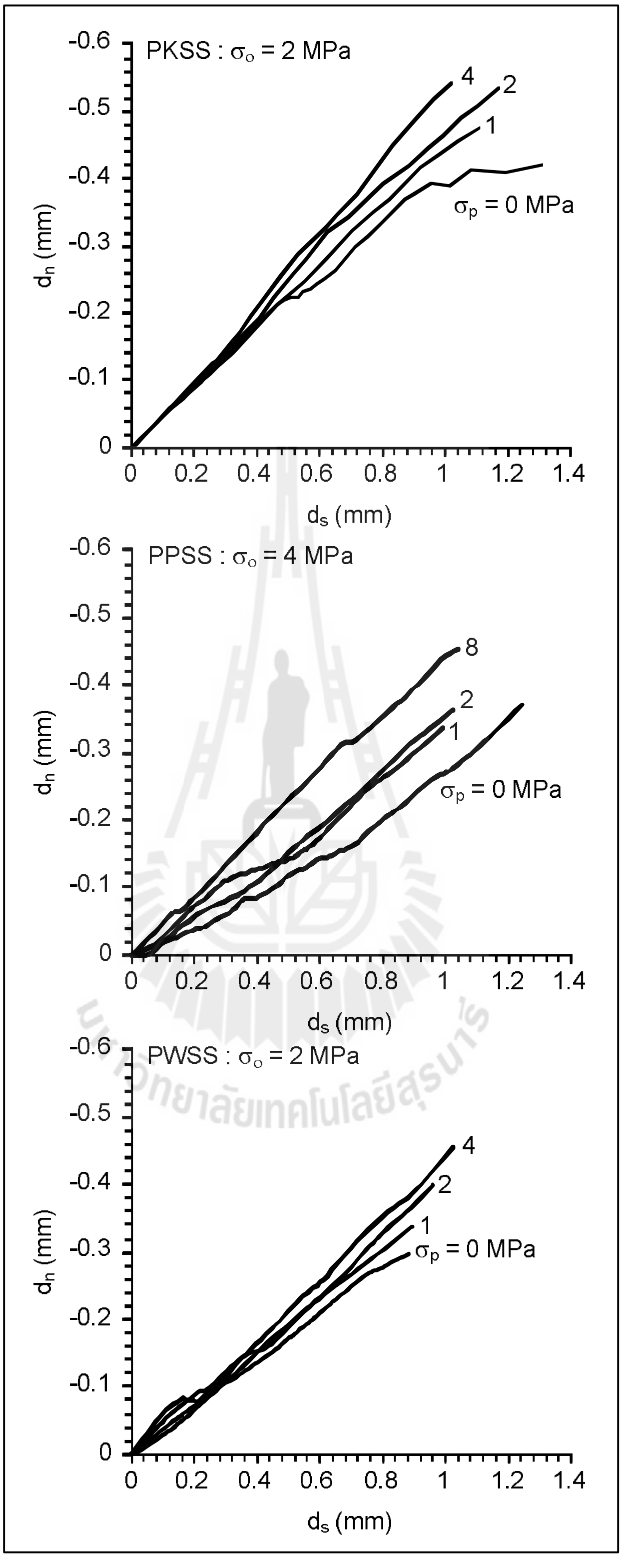

Figure 5.2 Normal displacement (d_n) as a function of shear displacement (d_s) for some specimens.

The maximum axial stresses (corresponding to the peak shear strengths) are plotted as a function of σ_o for various σ_p/σ_o ratios in Figure 5.3. The results indicate that the lateral stress parallel to the fracture plane (σ_p) can significantly reduce the fracture shear strengths in all tested sandstones.

Based on the Coulomb criterion a linear relation is proposed to represent the peak shear strengths under various σ_p/σ_o ratios as follows:

$$\tau = \sigma_n \tan(\phi^*) + c^* \tag{5.3}$$

where ϕ^* and c^* are defined here as the apparent friction angle and apparent cohesion of the fractures. This is primarily to avoid confusing with the fracture cohesion (c) and friction angle (ϕ) conventionally obtained from the direct shear test with constant normal stress The above equation is fitted to the experimental results in the forms of τ-σ_n diagram in Figure 5.4. For all sandstone types ϕ^* decreases with increasing lateral stress ratios (σ_p/σ_o), which can be best described by an exponential equation (Figure 5.5):

$$\phi^* = \alpha \exp[-\kappa(\sigma_p/\sigma_o)] \tag{5.4}$$

where α and κ are empirical constants. The apparent cohesions obtained from this test series tend to be independent of σ_p/σ_o ratio. They are averaged as 2.18, 2.96 and 3.14 MPa for PKSS, PPSS and PWSS. Post-test observations show that the sheared off areas for the fractures under higher lateral stress σ_p tend to be larger than those tested under lower σ_p. Figure 5.6 shows some post-test specimens.

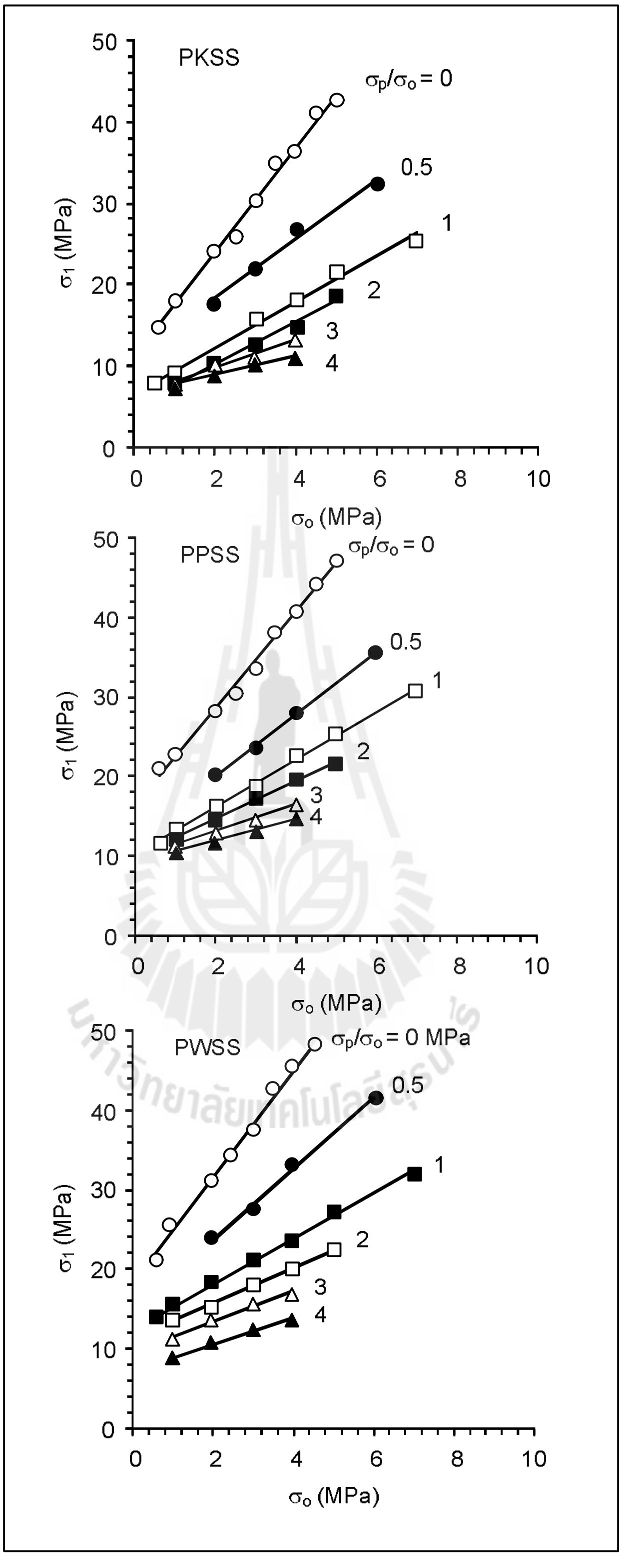

Figure 5.3. Major principal stresses (σ_1) corresponding to the peak shear strength as a function of lateral stress (σ_o) for various σ_p/σ_o ratios.

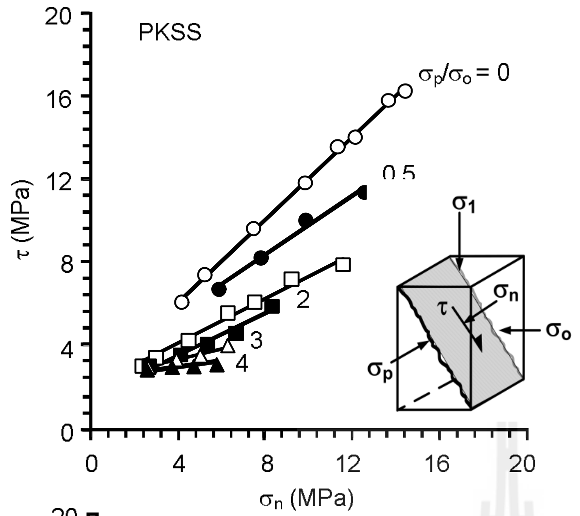

σ_p/σ_o (MPa)	$\tau = \sigma_n \tan \phi^* + c^*$		R^2
	ϕ^* (Degrees)	c^* (MPa)	
0	45	2.01	0.99
0.5	35	2.77	0.98
1	29	1.91	0.98
2	27	1.51	0.98
3	15	2.27	0.97
4	5	2.62	0.98
	$c^*_{average}$ =	2.18	

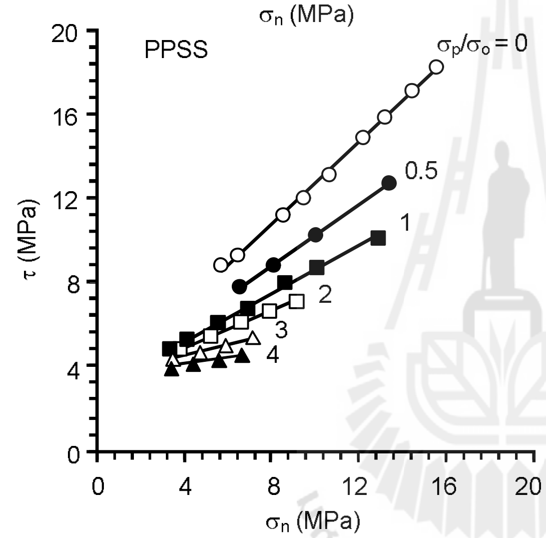

σ_p/σ_o (MPa)	$\tau = \sigma_n \tan \phi^* + c^*$		R^2
	ϕ^* (Degrees)	c^* (MPa)	
0	44	3.10	0.99
0.5	36	3.08	0.99
1	30	2.93	0.99
2	24	3.23	0.99
3	15	3.51	0.99
4	8	3.67	0.99
	$c^*_{average}$ =	3.25	

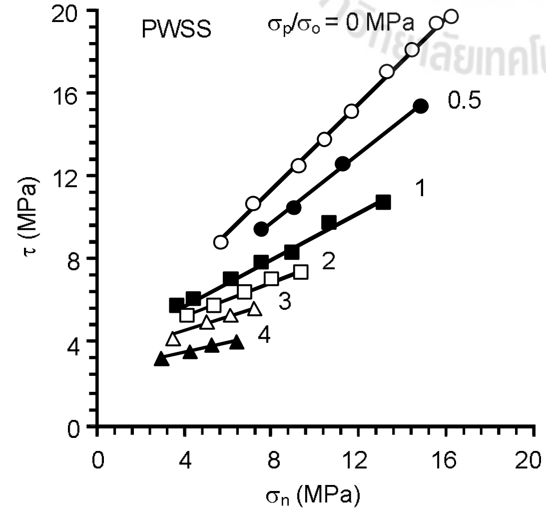

σ_p/σ_o (MPa)	$\tau = \sigma_n \tan \phi^* + c^*$		R^2
	ϕ^* (Degrees)	c^* (MPa)	
0	44	3.10	0.99
0.5	36	3.08	0.99
1	30	2.93	0.99
2	24	3.23	0.99
3	15	3.51	0.99
4	8	3.67	0.99
	$c^*_{average}$ =	3.25	

Figure 5.4 Peak shear strength (τ) as a function of normal stress (σ_n) for various σ_p/σ_o ratios.

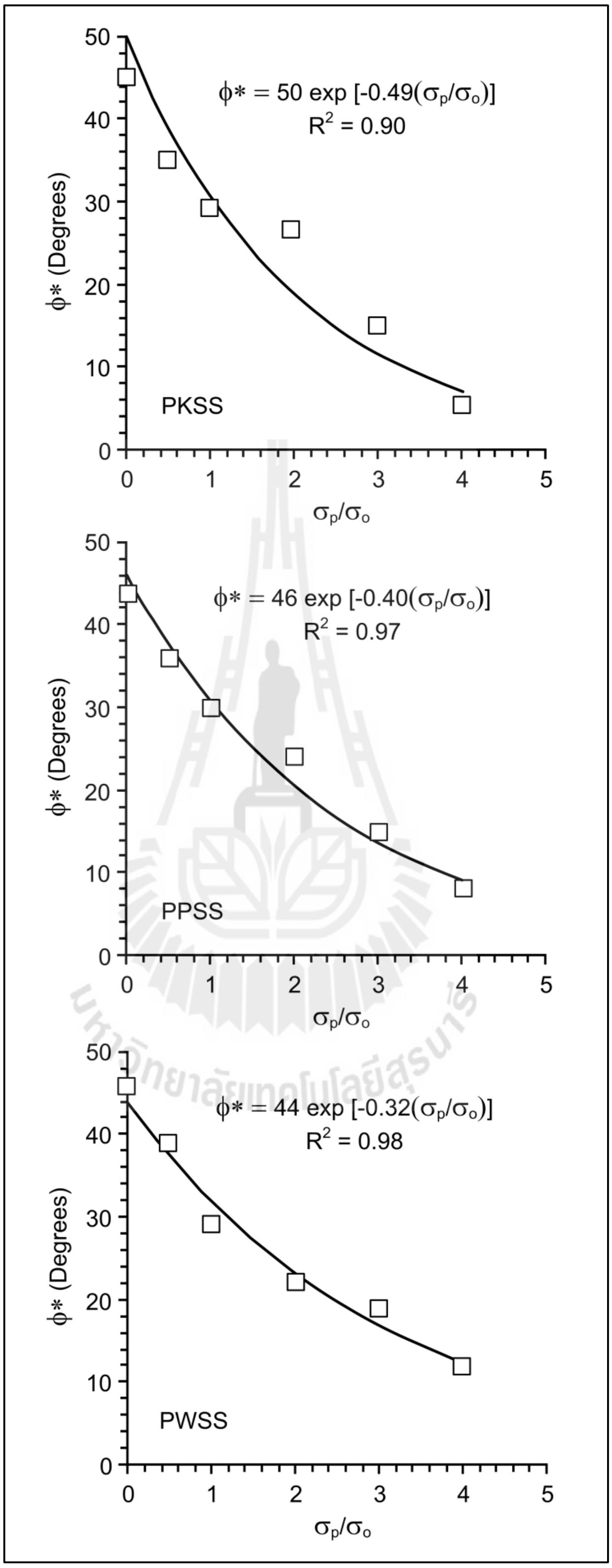

Figure 5.5 Apparent friction angles (ϕ*) as a function of σ_p/σ_o ratio.

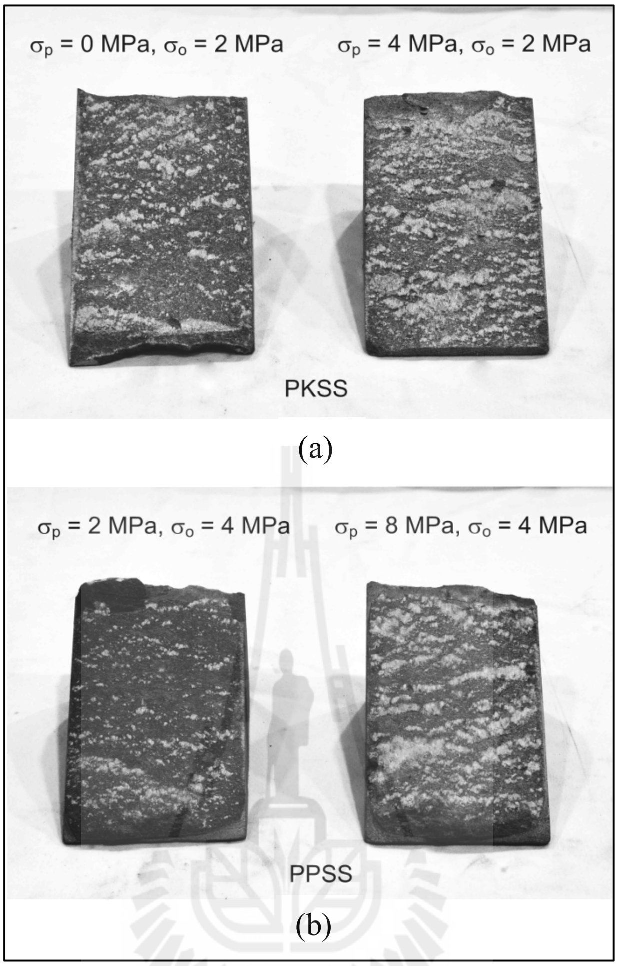

Figure 5.6 Some post-test fractures surface of PKSS (a) and PPSS (b).

5.2 Shear strength of tension-induced fractures under constant σ_p

The configurations of the sandstone specimens and test procedure for this test series are identical to those mentioned above. Here σ_p is maintained constant at 1, 2 and 3 MPa while σ_o is varied from 1.5 to 6 MPa. Table 5.2 summarizes the strength results. They are presented in the forms of τ-σ_n diagrams in Figure 5.7. For a comparison the true triaxial testing results at $\sigma_p = 0$ are also incorporated into the figure. It is found that the lateral stress σ_p can notably decrease the fracture shear strengths. A linear relation between the peak shear strengths and the normal stresses is obtained at all levels of σ_p which can also be represented by Eqs. 5.3. In this diagram ϕ^* tends to be independent of σ_p while c^* decreases exponentially as σ_p increases. The c^*- σ_p relation can be represented by:

$$c^* = \psi \exp [-\xi (\sigma_p)] \qquad (5.5)$$

where ψ and ξ are empirical constants. Their numerical values obtained from regression analysis are given in Figure 5.8. The apparent friction angles from the constant σ_p tests are averaged as 44°, 43° and 44°, for PKSS, PPSS and PWSS.

By substituting Eqs. (5.4) and (5.5) into (5.3) the following relation is obtained.

$$\tau = \sigma_n \tan \{\alpha \exp [-\kappa(\sigma_p/\sigma_o)]\} + \psi \exp [-\xi (\sigma_p)] \qquad (5.6)$$

Table 5.2 Summary of true triaxial shear strengths with constant σ_p at 1, 2 and 3 MPa.

σ_p (MPa)	σ_o (MPa)	PKSS			PPSS			PWSS		
		σ_1 (MPa)	σ_n (MPa)	τ (MPa)	σ_1 (MPa)	σ_n (MPa)	τ (MPa)	σ_1 (MPa)	σ_n (MPa)	τ (MPa)
1	1.5	14.52	4.75	5.64	17.50	5.50	6.93	20.78	6.32	8.35
	2	17.53	5.88	6.73	20.21	6.55	7.89	24.03	7.51	9.53
	2.5	22.17	7.41	8.52	24.80	8.07	9.66	29.21	9.18	11.57
	3	25.25	8.56	9.63	27.53	9.13	10.62	32.20	10.30	12.64
	3.5	27.86	9.59	10.55	31.78	10.57	12.25	35.07	11.40	13.67
	4	31.35	10.84	11.84	34.41	11.60	13.17	37.92	12.48	14.69
	4.5	34.41	11.98	12.95	35.95	12.36	13.62	40.79	13.57	15.72
	5	36.86	12.97	13.80	38.50	13.38	14.51	45.12	15.03	17.37
2	2.5	17.14	6.16	6.34	19.35	6.71	7.29	24.86	8.09	9.68
	3	20.34	7.33	7.51	23.34	8.09	8.81	27.89	9.22	10.78
	3.5	23.34	8.46	8.59	26.39	9.22	9.91	30.42	10.23	11.66
	4	27.14	9.79	10.02	27.89	9.97	10.34	33.19	11.30	12.64
	4.5	29.39	10.72	10.77	30.96	11.11	11.46	37.09	12.65	14.11
	5	31.45	11.61	11.45	34.02	12.26	12.57	40.14	13.78	15.21
3	4	22.08	8.52	7.83	23.63	8.91	8.50	30.45	10.61	11.45
	4.5	25.11	9.65	8.93	27.61	10.28	10.00	33.17	11.67	12.41
	5	27.50	10.63	9.74	29.98	11.25	10.82	35.74	12.69	13.31
	5.5	29.61	11.53	10.44	32.85	12.34	11.84	38.25	13.69	14.18
	6	32.20	12.55	11.35	35.46	13.37	12.76	41.45	14.86	15.35

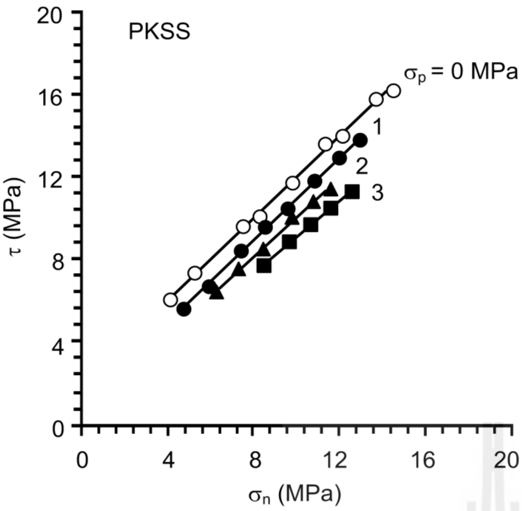

σ_p (MPa)	$\tau = \sigma_n \tan \phi^* + c^*$		R^2
	ϕ^* (Degrees)	c^* (MPa)	
0	45	2.00	0.99
1	45	0.95	0.99
2	44	0.53	0.99
3	42	0.54	0.99
$\phi^*_{average}$ = 44.0			

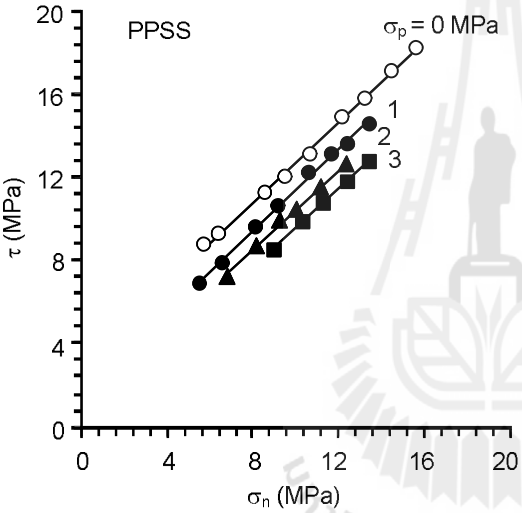

σ_p (MPa)	$\tau = \sigma_n \tan \phi^* + c^*$		R^2
	ϕ^* (Degrees)	c^* (MPa)	
0	44	3.10	0.99
1	44	1.62	0.99
2	43	1.18	0.99
3	43	0.17	0.99
$\phi^*_{average}$ = 43.5			

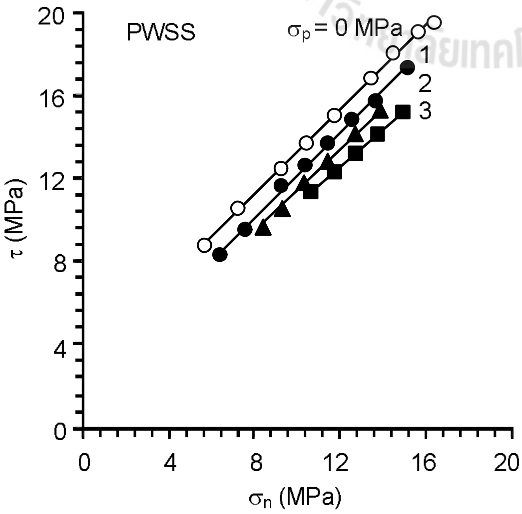

σ_p (MPa)	$\tau = \sigma_n \tan \phi^* + c^*$		R^2
	ϕ^* (Degrees)	c^* (MPa)	
0	46	3.13	0.99
1	46	1.90	0.99
2	44	1.77	0.99
3	42	1.79	0.99
$\phi^*_{average}$ = 44.5			

Figure 5.7 Peak shear strength (τ) as a function of normal stress (σ_n) for various σ_p.

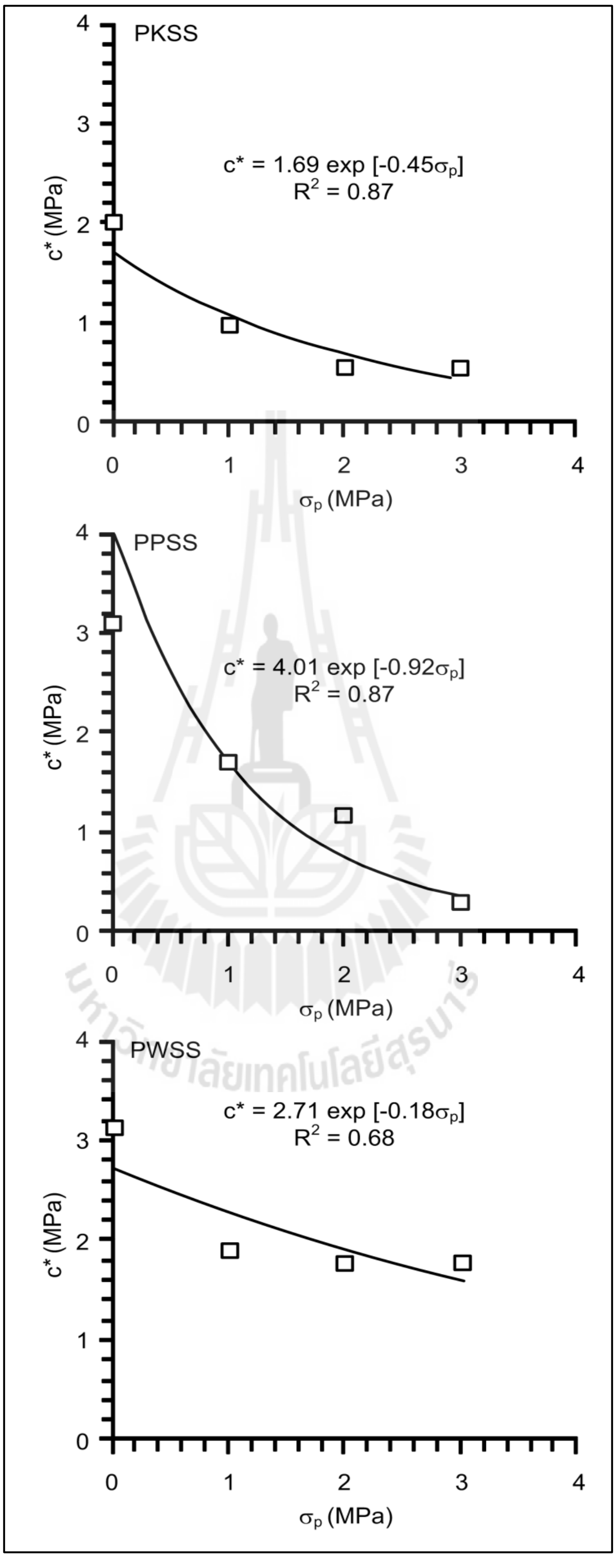

Figure 5.8 Apparent cohesion (ϕ*) as a function of σ_p.

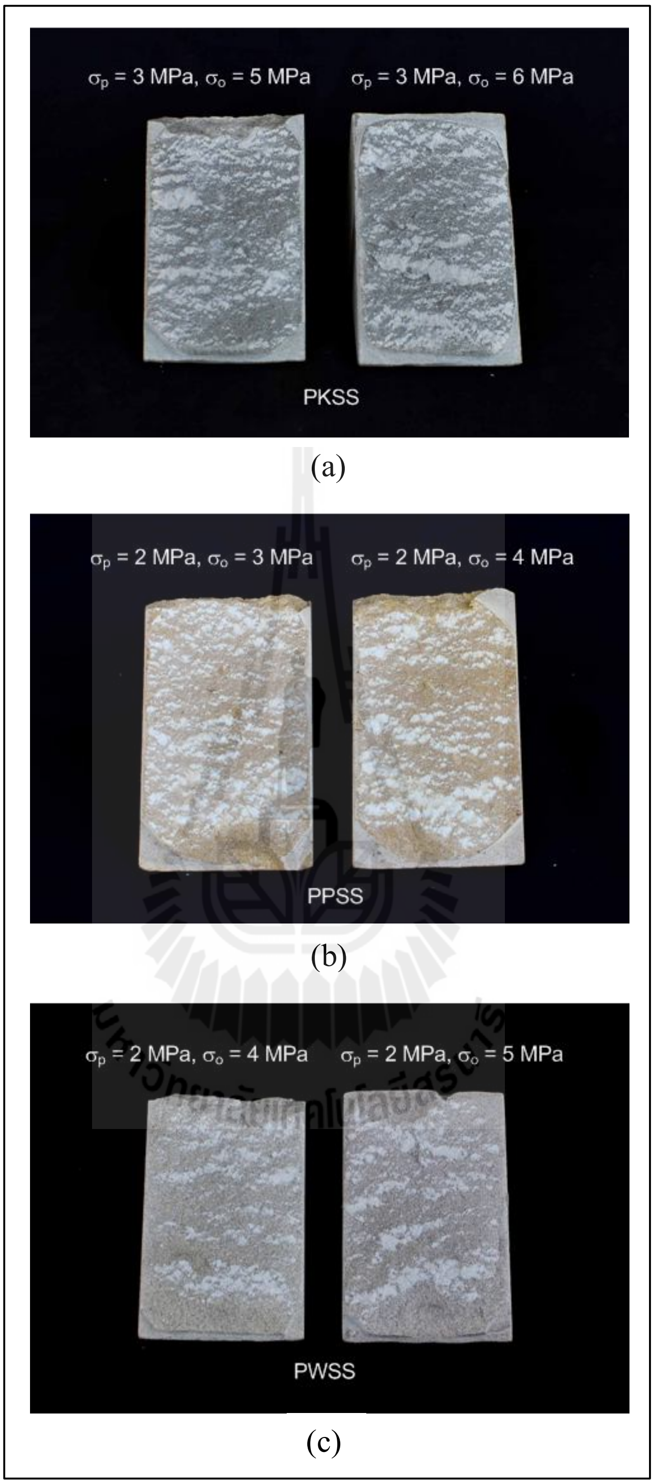

Figure 5.9 Some post-test fractures surface (σ_p constant) of PKSS (a), PPSS (b) and PWSS (c).

5.3 Shear strengths of saw-cut surfaces under constant lateral stress σ_p

This test series is performed to determine the σ_p effect on the shearing resistance of the smooth saw-cut surfaces. The test method and strength calculation are identical to those of the tension-induced fractures. The σ_p values are maintained constant at 0, 1 and 2 MPa, and the lateral stress σ_o varies from 2 to 10 MPa. Figure 5.10 shows the test results in the forms of τ-σ_n diagram where they are correlated well with the linear relation given by Eqs. 5.3. The shearing resistances for the smooth surfaces of the three tested sandstones tend to be independent of the lateral stress σ_p, as evidenced by the similar values of ϕ*and c* obtained from different magnitudes of σ_p. This indicates that the load correction for the frictional resistance (induced by σ_p) at the platen-neoprene interfaces is appropriate. It may be postulated that the effects of the lateral stress σ_p may relate to the fracture roughness, asperity amplitude and strength of the rock walls. More discussions on the σ_p effect are given in the following section. Figure 5.11 shows some post-test specimens.

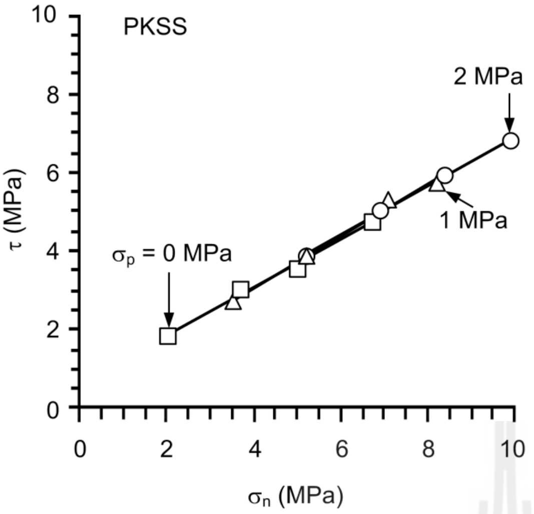

σp (MPa)	τ = σn tan ϕ* + c*		R^2
	ϕ* (Degrees)	c* (MPa)	
0	31	0.69	0.99
1	33	0.68	0.97
2	32	0.70	0.99
ϕ* average = 32°		c* average = 0.69	

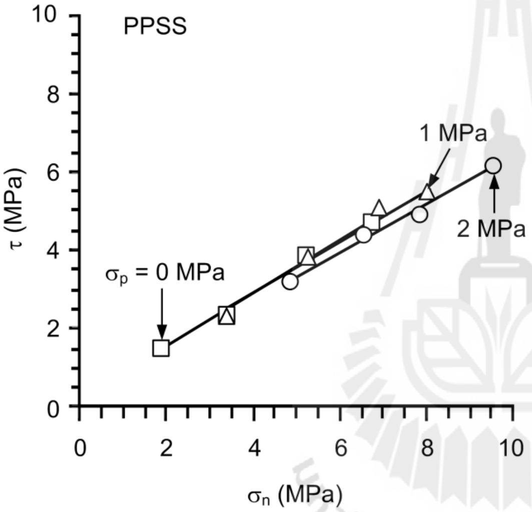

σp (MPa)	τ = σn tan ϕ* + c*		R^2
	ϕ* (Degrees)	c* (MPa)	
0	34	0.26	0.99
1	33	0.36	0.97
2	31	0.32	0.99
ϕ* average = 32°		c* average = 0.31	

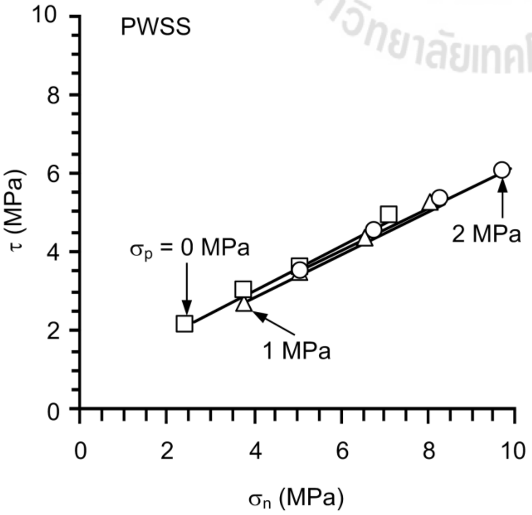

σp (MPa)	τ = σn tan ϕ* + c*		R^2
	ϕ* (Degrees)	c* (MPa)	
0	31	0.71	0.99
1	30	0.65	0.99
2	30	0.73	0.99
ϕ* average = 30°		c* average = 0.70	

Figure 5.10 Shear strengths of smooth saw-cut surfaces.

Figure 5.11 Some post-test saw-cut surface of PKSS PPSS and PWSS.

5.4 Direct shear tests

The direct shear tests are performed on the tension-induced fractures of the three sandstones to verify the reliability of the true triaxial test results above and to correlate the fracture shear strengths obtained from the two tests. The stress paths used for the two shear tests are different. For the true triaxial shear test both normal and shear stresses increase with the applied axial stress. For the direct shear test the normal stress is maintained constant during shearing (i.e. constant normal load test – CNL). The test method and calculation for the direct shear test follow the ASTM (D5607-08) standard practice. The shear force is increased until a total shear displacement of 10 mm is reached. The normal (dilation) and shear displacements are monitored using LVDT's (Figure 5.12). The constant normal stresses are 1, 2, 3 and 4 MPa. These normal stresses are lower than those used in the true triaxial shear test primarily due to the load limitations of the direct shear device and the polyaxial load frame. The maximum normal stress for the direct shear device is 4 MPa (for 100×100 mm^2 fracture area) while the possible minimum normal stress for the true triaxial shear test is about 5 MPa. Figure 5.13 shows some post-test specimens.

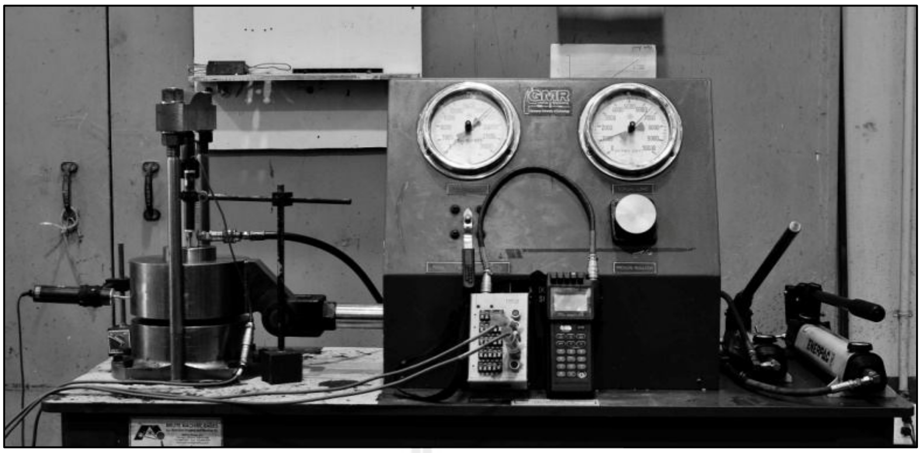

Figure 5.12 Direct shear machine SBEL DR44 used in this study.

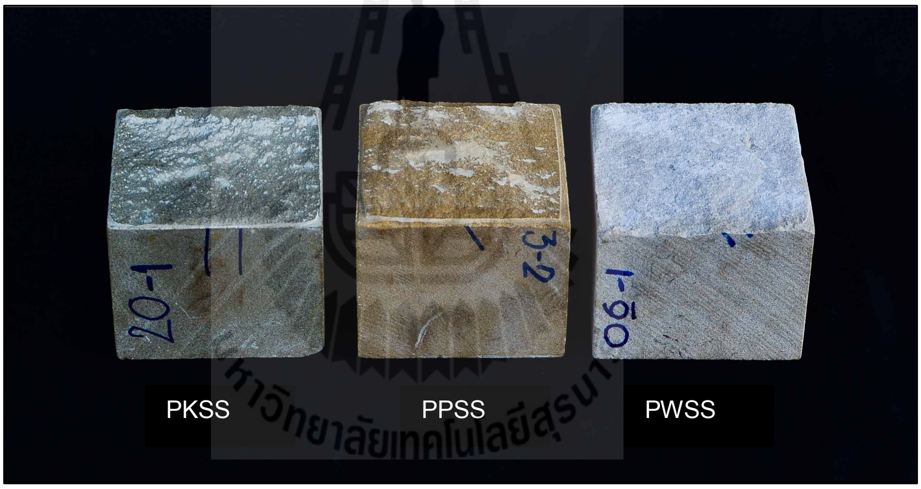

Figure 5.13 Some post-test direct shear of PKSS PPSS and PWSS.

Figure 5.14 shows the shear stresses and normal displacements as a function of shear displacement for all direct shear specimens. The direct shear strengths are compared with the true triaxial shear strengths under $\sigma_p = 0$ in Figure 5.15. Based on the Coulomb criterion both tests show similar cohesions and friction angles. Some discrepancies may be due to the intrinsic variability of the rock fractures. The results also suggest that under the range of the normal stresses used here different stress paths have insignificant impact on the peak shear strengths of the tension-induced fractures of the three sandstones.

Let us assume here that the peak shear strengths from both tests are the same for the condition where $\sigma_p = 0$, Eqs. (5.4), (5.5) and (5.6) reduce to

$$\phi^* = \alpha \tag{5.7}$$

$$c^* = \psi \tag{5.8}$$

$$\tau = \sigma_n \tan \{\alpha\} + \psi \tag{5.9}$$

Under unconfined condition the parameters α and ψ become the friction angle (ϕ) and cohesion (c) of the fracture. A more general form of Eq. (5.6) can be written as:

$$\tau = \sigma_n \tan \{ \phi \cdot \exp [-\kappa(\sigma_p/\sigma_o)]\} + c \cdot \exp [-\xi (\sigma_p)] \tag{5.10}$$

Eq. (5.12) allows a transition of the fracture shear strengths from the unconfined condition ($\sigma_p = 0$, direct shear testing) to the confined conditions ($\sigma_p > 0$, true triaxial shear testing).

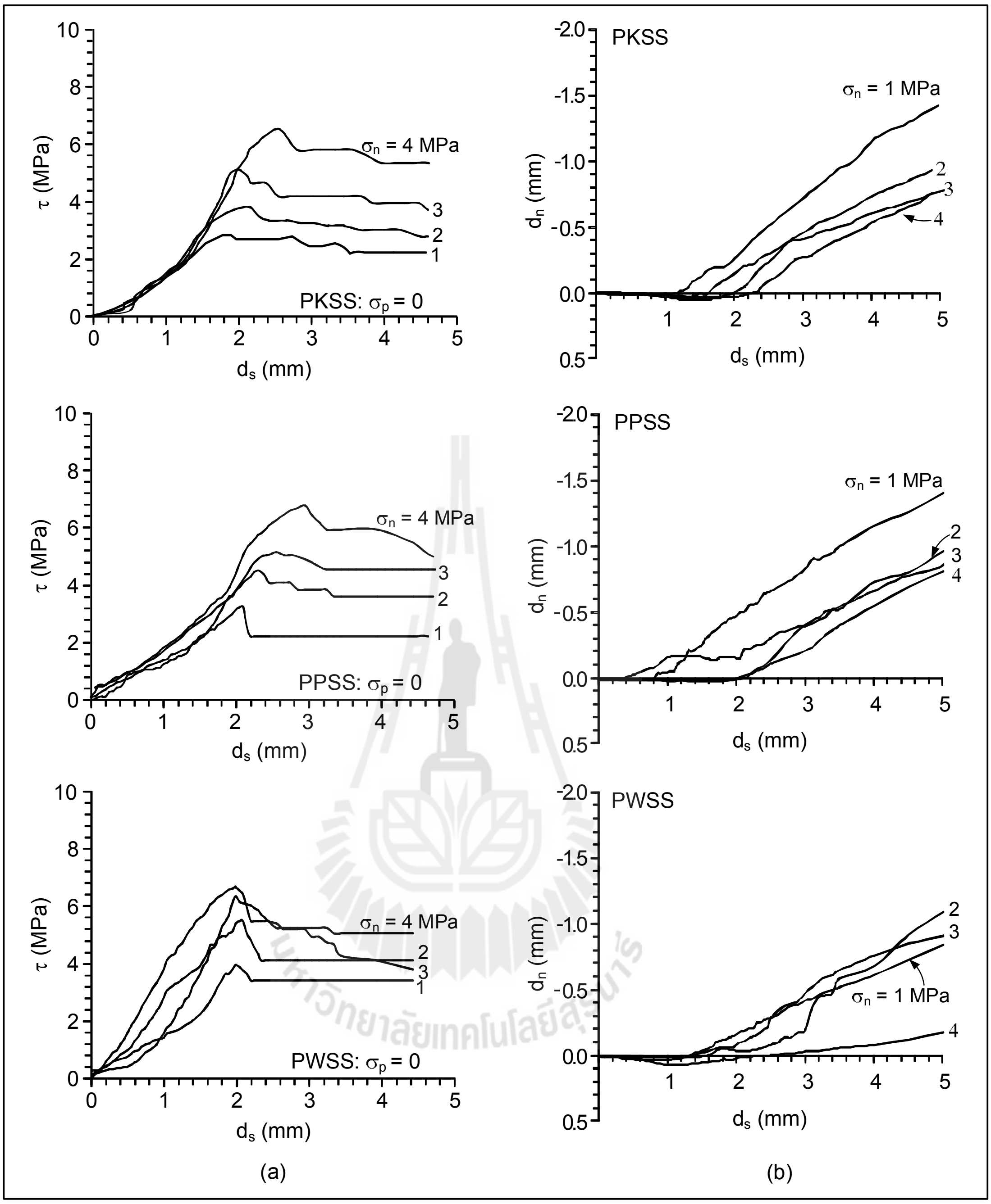

Figure 5.14 Direct shear test result: shear stress as a function of shear displacement (a), normal displacement as a function of shear displacement (b).

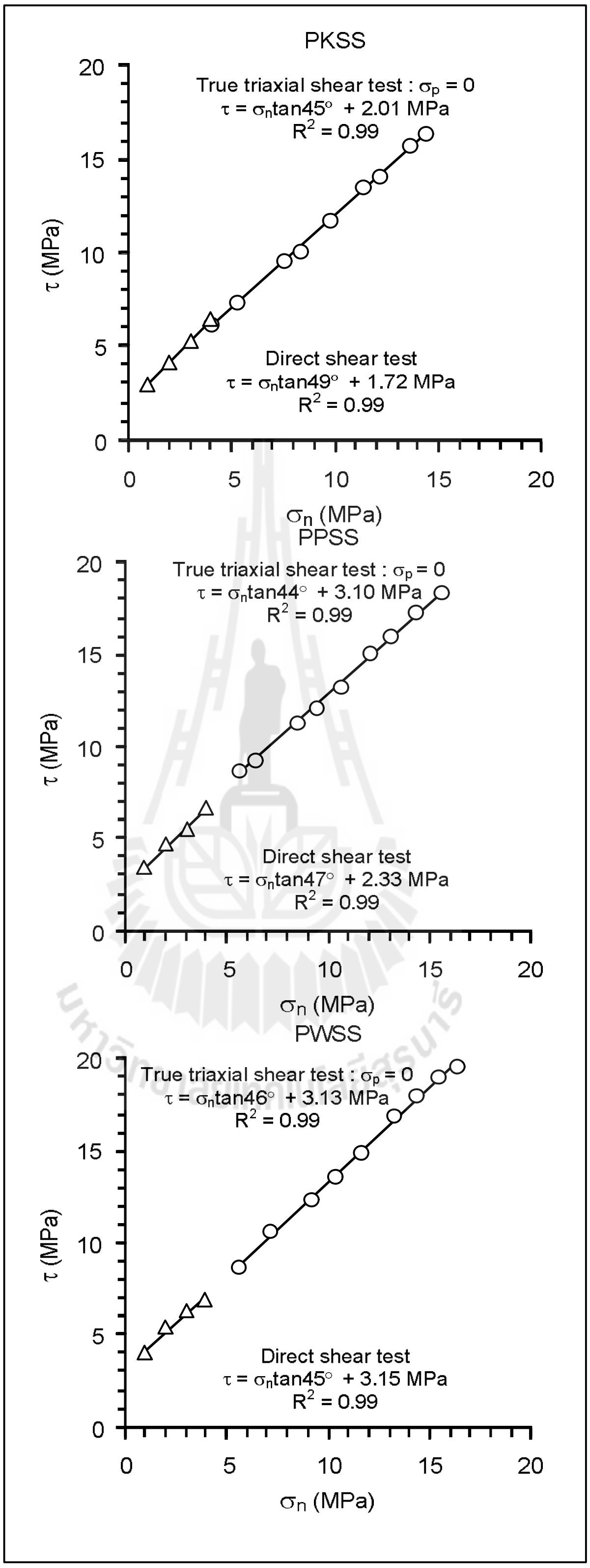

Figure 5.15 Direct shear tests results compared with true triaxial shear test results at $\sigma_p = 0$.

CHAPTER VI

DISCUSSIONS, CONCLUSIONS AND RECOMMENDATIONS FOR FUTURE STUDIES

6.1 Discussions and conclusions

From the results of this study it can be concluded that the lateral stress (σ_p) parallel to the sliding plane and perpendicular to the sliding direction can significantly reduce the cohesion and friction angle of the fractures. The greater magnitudes of the lateral stress σ_p result in larger sheared off areas and larger dilations. In general the decrease of the fracture cohesion with increasing confining pressures (for the case of lateral stress ratiso $\sigma_p/\sigma_o = 1$) as observed here agrees reasonably well with the experimental results obtained by Ramamurthy and Arora (1994). This means that the fracture shear strengths from the (unconfined) direct shear testing may not truly represented the fault or fracture shear strengths under the multi-axial stresses of in-situ conditions.

It is postulated that σ_p induces lateral tensile strains (dilation) of the rock asperities into the fracture aperture. These asperities can be sheared off more easily when the fractures are subject to shear load, and hence resulting in a lower frictional resistance. This is evidenced by the fact that σ_p has no effect on the shear strength of smooth saw-cut surfaces. The reduction of the cohesion and friction angle probably depends on the roughness characteristics (amplitudes, scale, and asperity strength). Fractures in other rocks, that have different surface roughness and strengths from those tested here, may exhibit different degrees of the σ_p-dependent shear strengths. Different shear strength criteria may be required to describe the results if the τ-σ_n relationship is non-linear. For other rock types different empirical forms may be used to represent the relations between the apparent friction angle and the lateral stress ratio (σ_p/σ_o) and between the apparent cohesion and the lateral stress σ_p. The exponential form used here has the advantage that it allows a transition of the shear strengths under unconfined condition (e.g., direct shear testing) to true triaxial stress states. The proposed relation is supported by the fact that the test results from the direct shear testing and from the true triaxial shear testing under $\sigma_p = 0$ are very similar. This suggests that the loading path has insignificant impact on fracture shear strengths in the tested sandstones.

6.2 Recommendations

The fractures tested here are relatively smooth (JRC = 6-8), small (76×148 mm^2), obtained from only three rock types with similar mechanical properties, and under a narrow range of the applied stresses. More testing is required on various rock types and fracture characteristics to further investigate the effects of fracture roughness, scale (e.g. Fardin et al., 2001), and strength of the asperities (e.g. Yang et al., 2001), and incorporate them into the proposed polyaxial shear strength criterion.

REFERENCES

Alexeev, A.D., Revva, V.N., Bachurin, L.L., Prokhorov, I.Y. (2008). The effect of stress state factor on fracture of sandstones under true triaxial loading. **International Journal of Fracture.** 149 (1): 1-10.

ASTM D5607-08. Standard test method for performing laboratory direct shear strength tests of rock specimens under constant normal force. **In Annual Book of ASTM Standards** (Vol. 04.08). Philadelphia: American Society for Testing and Materials.

Barton, N. (1982). Shear strength investigations for surface mining. **International Conference on Surface mining**. 171-196.

Barton N. R. (1997). The shear strength of rocks and rock joints. **International Journal of Rock Mechanics & Mining Sciences**. 34: 255-279.

Babanouri, N., Nasab, S.K., Baghbanan, A., Mohamadi, H.R. (2011). Over-consolidation effect on shear behavior of rock joints. **International Journal of Rock Mechanics & Mining Sciences**. 48 (8): 1283-1291.

Brady, B.H.G., Brown, E.T. (2006). **Rock Mechanics for Underground Mining** (3rd. Edn.). Springer, Netherlands, 628 p.

Fardin, N., Stephansson, O., Jing, L. (2001). The scale dependence of rock joint surface roughness. **International Journal of Mechanics and Mining Sciences**. 38, 659-669.

Fuenkajorn, K., Kenkhunthod, N. (2010). Influence of Loading Rate on Deformability and Compressive Strength of Three Thai Sandstones. **Geotechnical and Geological Engineering**. 28: 707-715.

Fuenkajorn, K., Sriapai, T.,Samsri, P. (2012) .Effects of loading rate on strength and deformability of MahaSarakham salt. **Engineering Geology**. 135-136, 10-23

Grasselli, G., Egger, P. (2003). Constitutive law for the shear strength of rock joints based on three-dimensional surface parameters. **International Journal of Rock Mechanics & Mining Sciences**. 40 (1): 25-40.

Haimson, B., Chang, C. (2000). A new true triaxial cell for testing mechanical properties of rock, and its use to determine rock strength and deformability of Westerly granite. **International Journal of Rock Mechanics & Mining Sciences**. 37 (1-2): 285-296.

Jaeger, J.C., Cook, N.G.W., Zimmerman, R.W. (2007). **Fundamentals of Rock Mechanics** (4th. Edn.). Blackwell Publishing, Malden, 475 p57.

Hoek E, Brown E. (1997). Practical estimates of rock mass strength. **International Journal of Rock Mechanics & Mining Sciences**. 34 (8): 1165-86.

Kusumi, H., Teraoka, K., Nishida, K. (1997). Study on new formulation of shear strength for irregular rock joints. **International Journal of Rock Mechanics & Mining Sciences**. 34 (3-4): 168.e1-168.e15.

Ladanyi B., Archambault G. (1997). Simulation of shear behaviour of a jointed rock mass. **Proceedings of the 11 th Symposium of Rock Mechanics**. AIME

Maksimovic, M. (1996). The shear strength components of a rough rock joint. International **Journal of Rock Mechanics and Mining Sciences & Geomechanics Abstracts**. 33 (8): 769-783.

Ramamurthy, T., Arora, V.K. (1994). Strength predictions for jointed rocks in confined and unconfined states. **International Journal of Mechanics and Mining Sciences and Geomechanics Abstracts**. 31 (1), 9-22.

Rao, K.S., Tiwari, R.P. (2008). A polyaxial system for testing of jointed rock mass models. **Geotechnical Testing Journal**. 31 (4): 285-294.

Singh, B., Goel, R.K., Mehrotra, V.K., Garg, S.K., Allu, M.R. (1998). Effect of intermediate principal stress on strength of anisotropic rock mass. **Tunnelling and Underground Space Technology**. 13 (1): 71-79.

Yang, Z.Y., Di, C.C., Yen, K.C., 2001. The effect of asperity order on the roughness of rock joints. **International Journal of Mechanics and Mining Sciences**. 38, 745-752.

Zhao, J. (1997). Joint surface matching and shear strength part b: JRC-JMC shear strength criterion. **International Journal of Rock Mechanics & Mining Sciences**. 34 (2): 179-185.

APPENDIX A

SHEAR-DISPLACEMENT AND NORMAL-SHEAR DISPLACEMENT CURVES

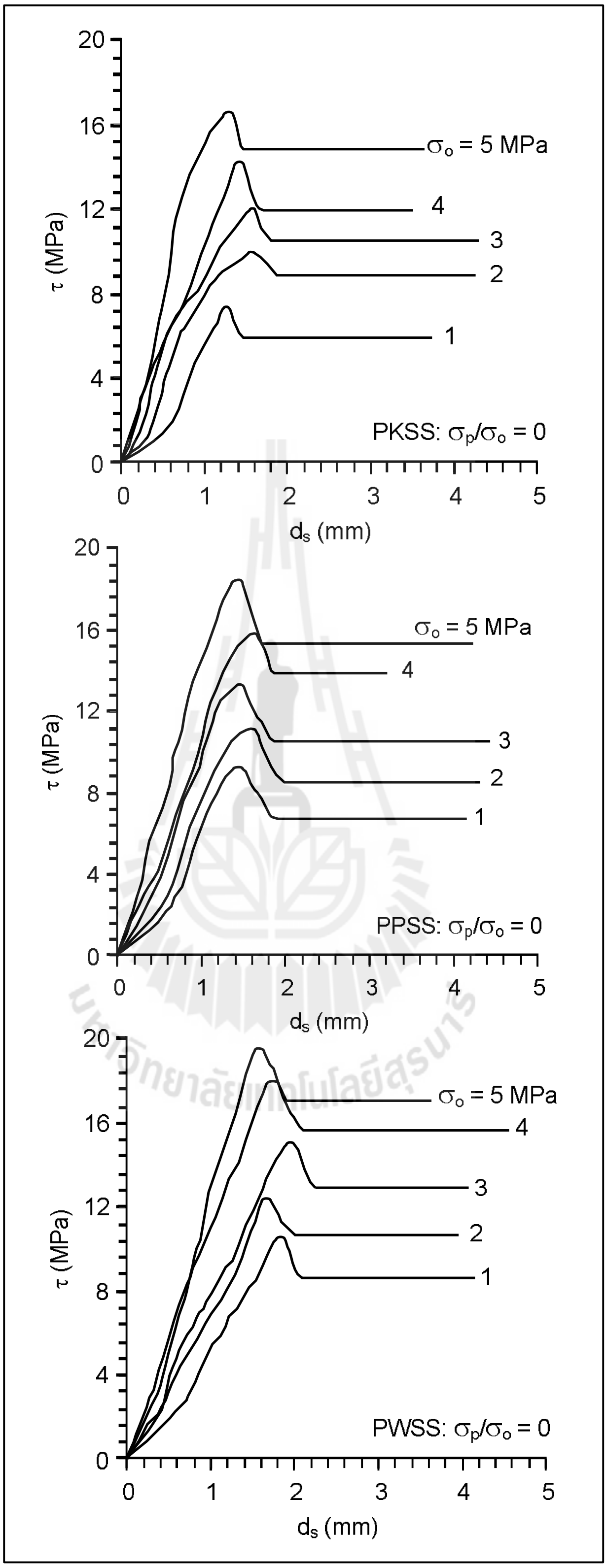

Figure A-1 Shear stresses (τ) as a function of shear displacement (d_s) for some σ_p/σ_o ratios = 0.

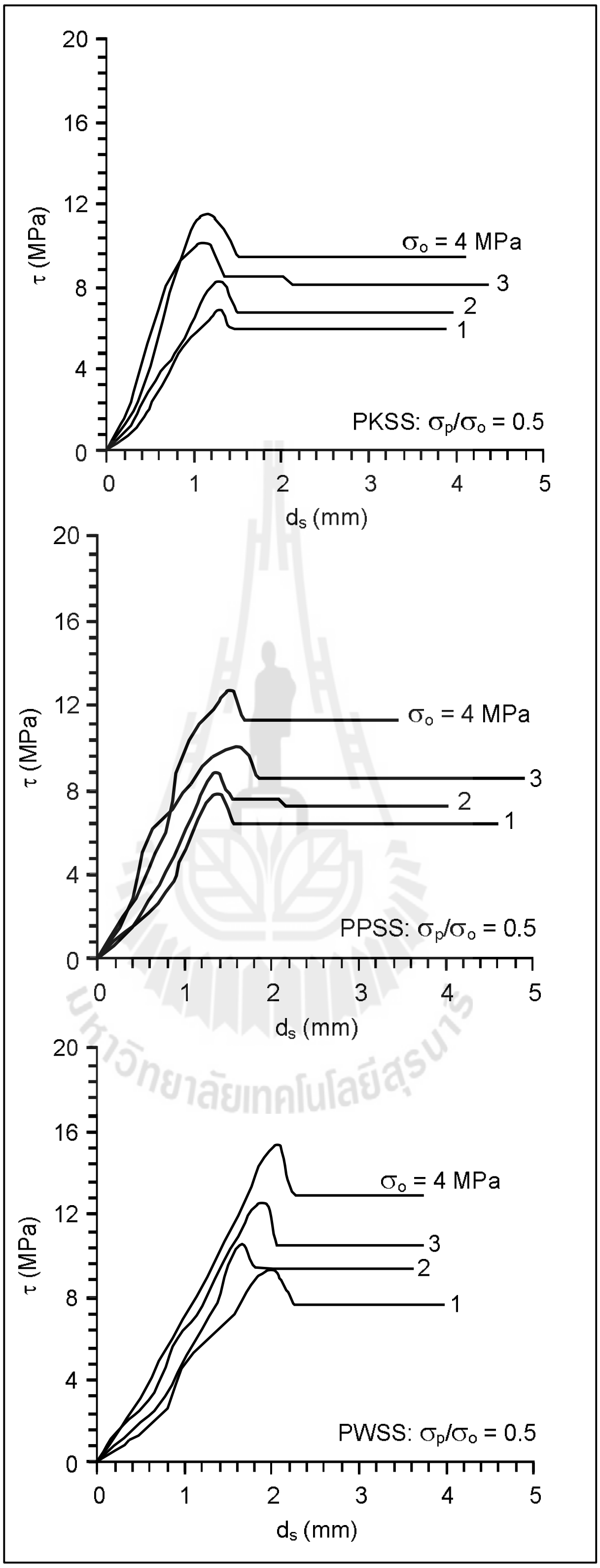

Figure A-2 Shear stresses (τ) as a function of shear displacement (d_s) for some σ_p/σ_o ratios = 0.5.

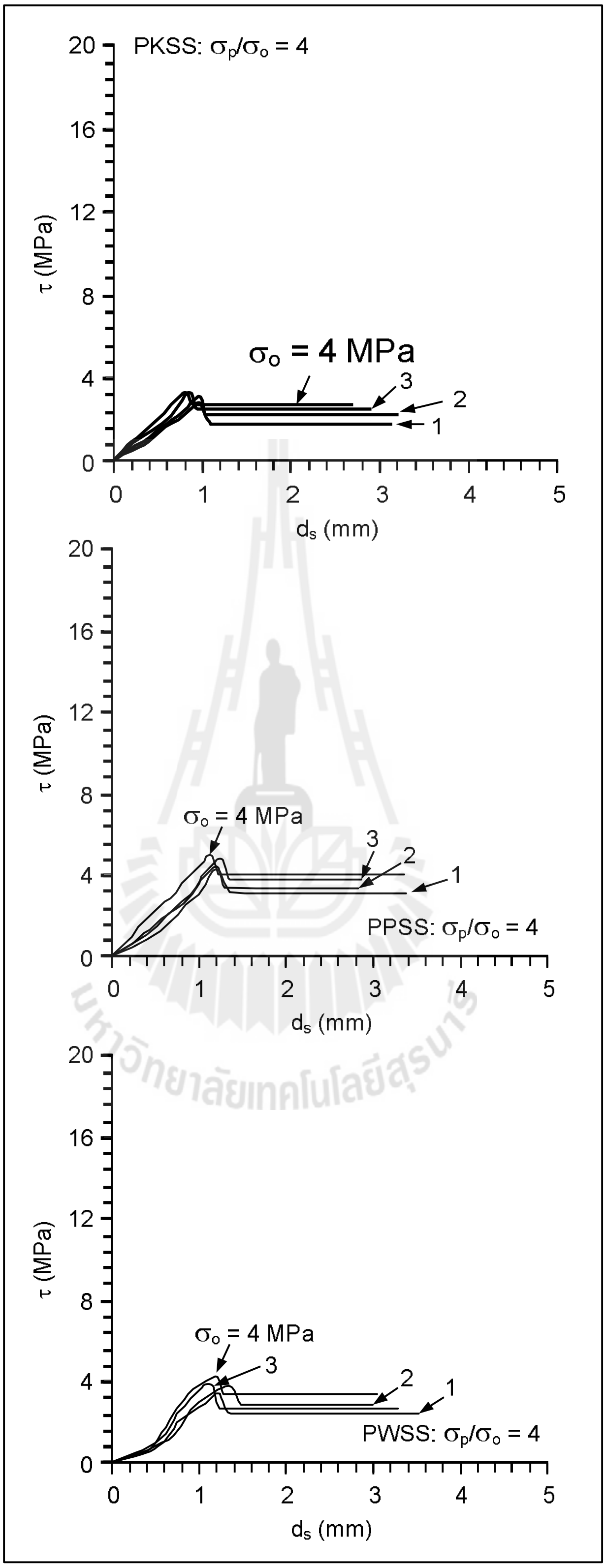

Figure A-3 Shear stresses (τ) as a function of shear displacement (d_s) for some σ_p/σ_o ratios = 4.

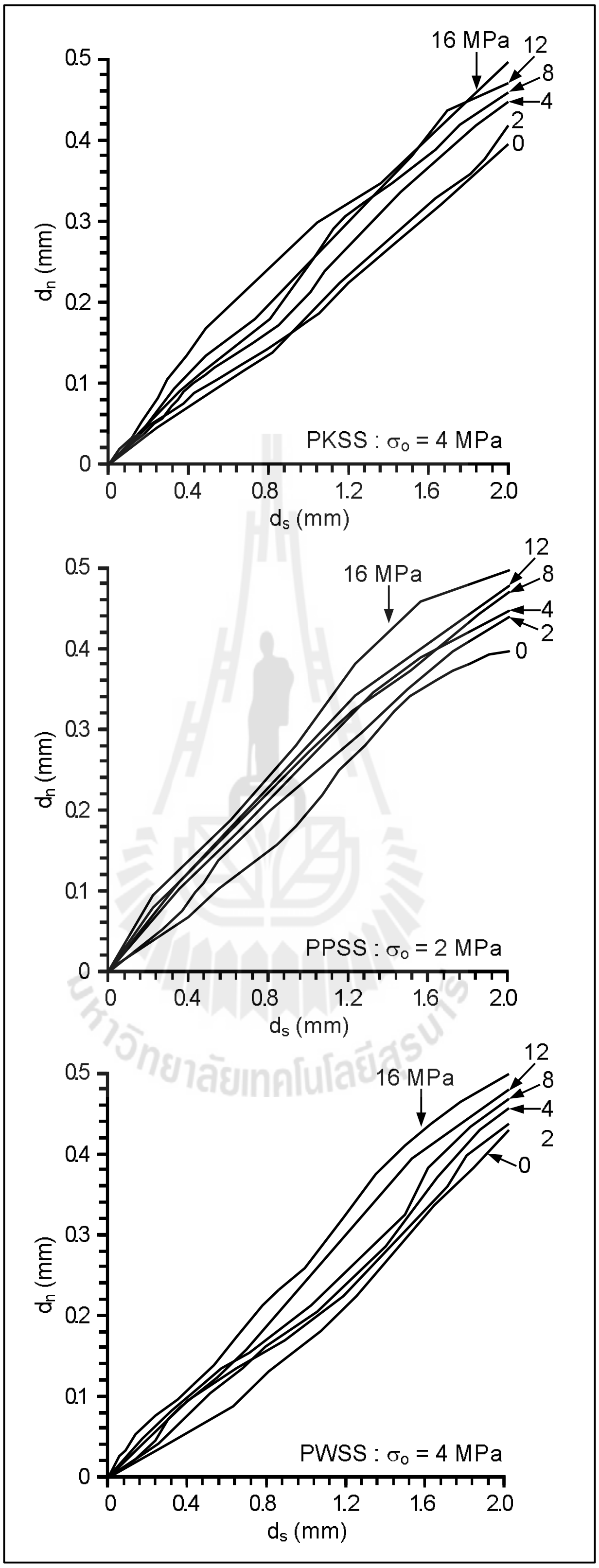

Figure A-4 Normal displacement (d_n) as a function of shear displacement (d_s) for some specimens (from condition σ_p/σ_o ratios).

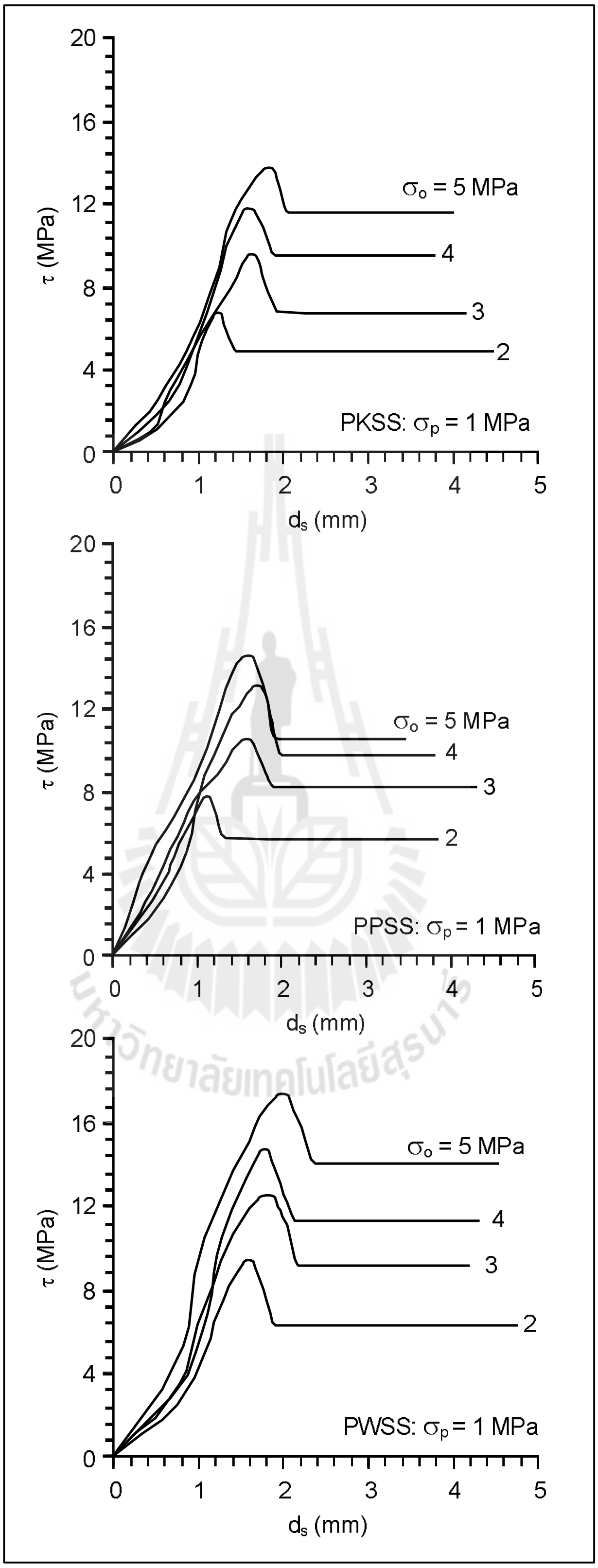

Figure A-5 Shear stresses (τ) as a function of shear displacement (d_s) for some constants σ_p.

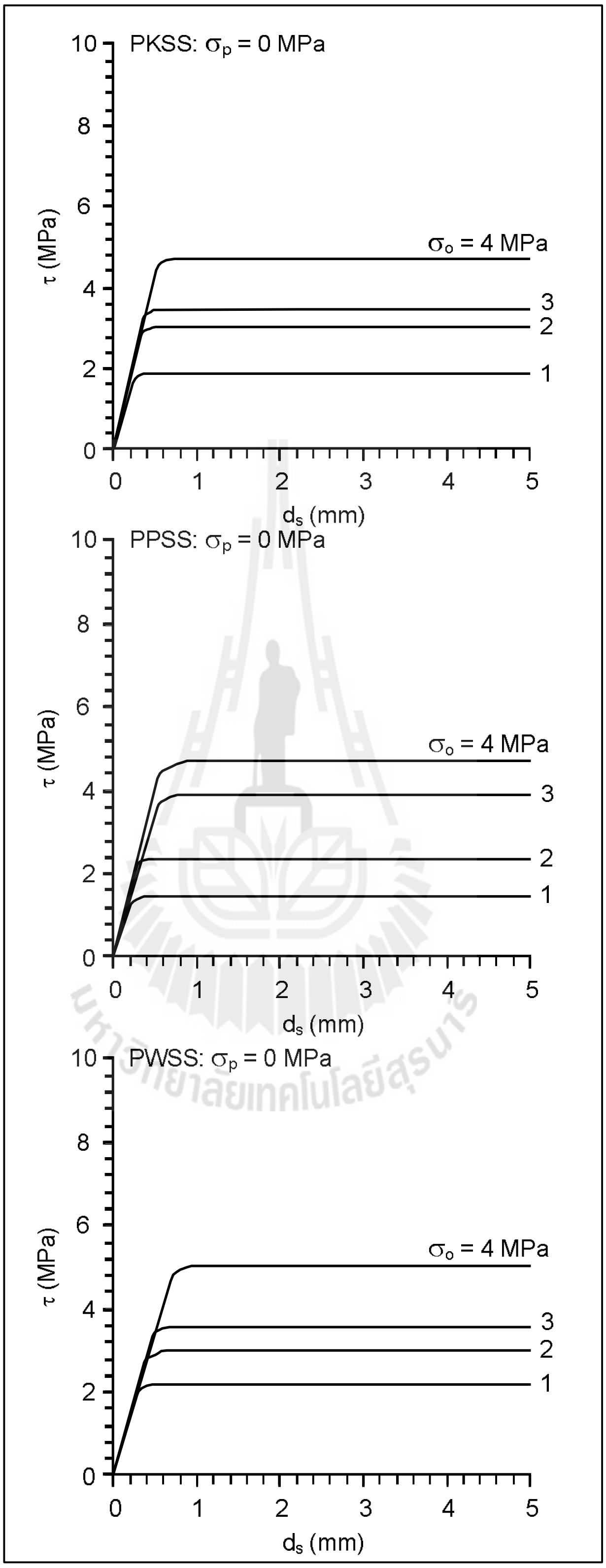

Figure A-6 Shear stresses (τ) as a function of shear displacement (d_s) for some specimens (condition of saw-cut surfaces).

BIOGRAPHY

Mr. Piyanat Kapang was born on October 17, 1987 in Ubon Ratchathanee province, Thailand. He received his Bachelor's Degree in Engineering (Geotechnology) from Suranaree University of Technology in 2010. For his post-graduate, he continued to study with a Master's degree in the Geological Engineering Program, Institute of Engineering, Suranaree university of Technology. During graduation, 2010-2012, he was a part time worker in position of research assistant at the Geomechanics Research Unit, Institute of Engineering, Suranaree University of Technology.